

Molecular Mechanism of TMEM16A Regulation: Role of CaMKII and PP1/PP2A

¹Ayon, R. J., ^{2,3}Hawn, M. B., ^{2,3}Aoun, J., ²Wiwchar, M., ²Forrest, A. S., ²Cunningham, F.,
²Singer, C.A., ²Valencik, M. L., ⁴Greenwood, I. A., and ^{2,3}N. Leblanc

¹Division of Translational and Regenerative Medicine, Department of Medicine, College of Medicine, The University of Arizona College of Medicine, Tucson, Arizona, USA
Arizona Health Sciences Center, ²Department of Pharmacology and ³The Center for Cardiovascular Research, Center of Biomedical Research Excellence for Molecular and Cellular Signal Transduction in the Cardiovascular System, University of Nevada, Reno School of Medicine, Reno, Nevada, USA, and ⁴Institute of Molecular & Clinical Sciences, St George's, London, UK

Running Head: *Regulation of TMEM16A by CaMKII and PP1/PP2A*

Corresponding Author:

Normand Leblanc, Ph.D.
Professor, Department of Pharmacology/MS 318
University of Nevada, Reno School of Medicine
Manville Health Sciences Building, Room 9D
1664 North Virginia Street
Reno, Nevada 89557-0318
U.S.A
Phone: 775-784-1420
Fax: 775-784-1620
Email: nleblanc@unr.edu

ABSTRACT

This study explored the mechanism by which Ca^{2+} -activated Cl^- channels (CaCC) encoded by the *Tmem16a* gene are regulated by CaMKII and protein phosphatases 1 (PP1) and 2A (PP2A). Ca^{2+} -activated Cl^- currents (I_{ClCa}) were recorded from HEK-293 cells expressing mouse TMEM16A. I_{ClCa} were evoked using a pipette solution in which free Ca^{2+} concentration ($[\text{Ca}^{2+}]_i$) was clamped to 500 nM, in the presence (5 mM) or absence of ATP. With 5 mM ATP, I_{ClCa} decayed to below 50% of the initial current magnitude within 10 min after seal rupture. I_{ClCa} rundown seen with ATP-containing pipette solution was greatly diminished by omitting ATP. I_{ClCa} recorded after 20 min of cell dialysis with 0 ATP were more than 2-fold larger than those recorded with 5 mM ATP. Intracellular application of autocamtide-2-related inhibitory peptide (5 μM) or KN-93 (10 μM), two specific CaMKII inhibitors, produced a similar attenuation of TMEM16A rundown. In contrast, internal application of okadaic acid (30 nM) or cantharidin (100 nM), two non-selective PP1 and PP2A blockers, promoted the rundown of TMEM16A in cells dialyzed with 0 ATP. Mutating Serine 528 of TMEM16A to an Alanine led to a similar inhibition of TMEM16A rundown to that exerted by either one of the two CaMKII inhibitors tested, which was not observed for three putative CaMKII consensus sites for phosphorylation (T273, T622 and S730). Our results suggest that TMEM16A-mediated CaCCs are regulated by CaMKII and PP1/PP2A. Our data also suggest that Serine 528 of TMEM16A is an important contributor to the regulation of I_{ClCa} by CaMKII.

INTRODUCTION

Ca²⁺-activated Cl⁻ currents (I_{ClCa}) recorded from many cell types have been shown to exhibit rundown following membrane rupture in the whole-cell recording mode or after patch excision to monitor single CaCC activity, which led investigators to speculate that the channels are the target of post-translational regulation (15, 22, 23, 29, 33). Wang and Kotlikoff (46) demonstrated for the first time that the rundown of I_{ClCa} in airway smooth muscle cells was attributed to phosphorylation involving the serine-threonine kinase calmodulin-dependent protein kinase II (CaMKII). A later study by our group showed that CaMKII-induced phosphorylation similarly reduced I_{ClCa} in rabbit coronary and pulmonary arterial smooth muscle cells but not in portal vein myocytes (13). In accordance with the hypothesis that CaCCs in arterial smooth muscle cells are regulated by phosphorylation was the demonstration that the rundown of I_{ClCa} was: 1) reversed by omitting ATP in the pipette solution or by replacing the nucleotide with a non-hydrolyzable form of ATP, AMP-PNP (1, 2, 47); and 2) antagonized by the Ca²⁺-dependent serine-threonine protein phosphatase Calcineurin (2, 14, 24), and protein phosphatases 1 and 2A (2). Because CaCCs exert a powerful depolarizing stimulus that can sustain Ca²⁺ influx through L-type Ca²⁺ channels (Ca_L) that itself reinforces CaCC activation, it is hypothesized that Ca²⁺-dependent down-regulation by CaMKII-induced phosphorylation may offer a means to attenuate the impact of the positive feedback loop between Ca_L and CaCCs (13, 22, 23, 36).

The discovery of the *Tmem16* or *Anoctamin* gene family encoding for CaCCs by three independent groups (5, 34, 49) paved the way for the molecular characterization of their biophysical properties, molecular assembly and membrane topology, functional role and regulation in various cell types. The first two members of this family of ten

paralogs, TMEM16A (or ANO1) and TMEM16B (Anoctamin-2 or ANO2), are confirmed CaCC pore-forming subunits whose properties resemble those of CaCCs characterized in native cells (16, 22, 31, 43). While the expression of ANO2 is low in VSMCs (7), TMEM16A is abundantly expressed in these cells and is believed to be the major CaCC contributing to I_{Ca} and its impact on the membrane depolarization and contraction of VSMCs mediated by endogenous vasoconstrictors (7, 8, 11, 17, 22, 26, 38, 41, 45).

The molecular mechanism(s) responsible for the regulation and more specifically the rundown of TMEM16A remains largely undefined. A recent study provided evidence that Serine 727 of mouse TMEM16A is the target amino acid responsible for the down-regulation of CaCCs by CaMKII γ in basilar artery smooth muscle cells, a post-translational modification suggested to be involved in regulating smooth muscle cell growth in cerebral blood vessels in an animal model of systemic hypertension (25). The goals of the present study were: 1) to assess whether TMEM16A-induced I_{Ca} is regulated by ATP, CaMKII and PP1/PP2A in a manner analogous to that of CaCCs in arterial myocytes (2, 13, 14, 24, 47); and 2) to identify the amino acid residue(s) that may be targeted by CaMKII and responsible, at least in part, for TMEM16A-induced CaCC inhibition by phosphorylation.

MATERIAL AND METHODS

Cell Culture

HEK-293 cells (ATCC, Manassas, VA) were maintained in Dulbecco's Modified Eagle Medium (DMEM; Thermo Fisher Scientific, Waltham, MA) with 10% (v/v) heat-inactivated fetal bovine serum (Thermo Fisher Scientific), and 1% (v/v) penicillin/streptomycin (Thermo Fisher Scientific). All cells were incubated in a

humidified environment containing 5% CO₂ at 37°C. Once the cells were 80 – 100% confluent, they were then trypsinized with 0.05% trypsin-EDTA (Thermo Fisher Scientific), and plated into T25 cell culture flasks to maintain the cell line for transient transfections of mouse TMEM16A for electrophysiological experiments.

Immunocytochemical Staining and Confocal Microscopy Imaging

Non-transfected HEK-293 cells grown on collagen I coated cover glass slips (Neuvitro Corporation, Vancouver, WA) were fixed with 4% paraformaldehyde in phosphate buffer saline (PBS) for 10 min at room temperature. After washing in PBS, the cells were blocked and permeabilized with 1% (w/v) bovine serum albumin (BSA) and 0.01% Triton X-100 (Sigma-Aldrich, St. Louis, MO) in PBS for 1 hour before incubation overnight at 4°C with primary goat polyclonal antibodies to PP1 α (Santa Cruz Biotechnology, Dallas, TX, sc-6105), PP1 β (Santa Cruz Biotechnology, sc-6107), PP1 γ (Santa Cruz Biotechnology, sc-6109) or rabbit monoclonal PP2A (Cell Signaling Technology, 52F8, Danvers, MA) and rabbit polyclonal CaMKII (Santa Cruz Biotechnology, sc-9035). For control experiments (2nd antibody only), the primary antibody was omitted. After washing repeatedly with PBS, the coverslips were subsequently incubated with goat anti-rabbit-IgG Alexa Fluor® 546 (Invitrogen; A-11010) or donkey anti-goat-IgG Alexa Fluor® 488 (Invitrogen; A-21447) diluted in blocking buffer (1:500) for 1h at room temperature and washed again in PBS. Fluoroshield mounting medium with 4',6-diamino-2-phenylindole (DAPI) (Abcam, Cambridge, UK) was used to mount coverslips onto precleaned microscope slides. Control slides were processed using secondary antibodies only. Slides were viewed and photographed using an Olympus FluoView FV 1000 laser scanning confocal microscope with an Olympus 60X PlanApo_N 1.42 NA oil immersion objective. DAPI

and secondary antibodies were visualized using 405 nm and 488 or 546 lines, respectively.

Western Blot Analysis

Non-transfected HEK-293 cells were collected and lysed in RIPA lysis buffer containing a cocktail of protease inhibitors. Proteins were separated in 4-12% NuPAGE (Thermo Fisher Scientific) and transferred into nitrocellulose membranes (0.45 μ m; BIORAD, Cat. # 162-0215). The membranes were blocked with LI-COR Odyssey blocking buffer (Lincoln, NB, Part no. 92740000) in PBS (1:1) for 1h at room temperature and incubated overnight at 4°C with the following primary antibodies (all diluted 1:1000 in LI-COR Odyssey blocking buffer in PBS (1:1) with 0.01% Tween-20): rabbit polyclonal CaMKII (Santa Cruz Biotechnology, Dallas, TX; sc-9035), rabbit monoclonal PP2A (Cell Signaling Technology, Danvers, MA, 52F8D8), goat polyclonal PP1 α (Santa Cruz Biotechnology, sc-6105), goat polyclonal PP1 β (Santa Cruz Biotechnology, sc-6107), or goat polyclonal PP1 γ (Santa Cruz Biotechnology, sc-6109), and rabbit polyclonal GAPDH (Santa Cruz Biotechnology, sc-25778) or goat polyclonal β -Actin (Santa Cruz Biotechnology, sc-1616). The membranes were incubated with Alexa Fluor 680 or 800 conjugated goat anti-rabbit IgG or donkey anti-goat (diluted 1:25,000 in LI-COR Odyssey blocking buffer in PBS (1:1) with 0.01% Tween-20) for 1h at room temperature. Signals were detected using Odyssey Infrared Imaging System (LI-COR) near infrared wavelengths using the 700 nm and 800 nm channels. All experiments were performed in triplicate.

RNA Isolation and cDNA Synthesis from HEK-293 Cells

mRNA was isolated from cultured non-transfected HEK-293 cells using PureZol (Bio-Rad, Hercules, CA). Prior to preparing cDNA, RNA was treated with DNase I

(Invitrogen, Grand Island, NY) to prevent genomic DNA contamination. cDNA was prepared using oligo(dT) and dNTP mixtures with Superscript III (Invitrogen). PCR primers were designed against the association domain for all four isoforms of CaMKII (α , β , γ , δ) and all primer sets spanned multiple exons (Table 1). All primers were synthesized by Integrated DNA Technologies (Coralville, IA). Amplification of cDNA was performed using GoTaq[®] Hot Start Polymerase (Promega, Madison, WI), which had an amplification profile consisting of an initial step to 95°C for 2 min to activate the Amplitaq polymerase, followed by 36 cycles of denaturation at 95°C for 30 s, annealing at Ta (in °C; the optimal annealing temperature for each primer pair; range: 60-63°C) for 30 s, and extension at 72°C for 5 min. The amplified products (10 μ l) were separated by electrophoresis on a 2% agarose/Tris, acetic acid, EDTA gel, and the DNA bands were visualized by ethidium bromide staining. A non-template control for the master mix of reagents made for each primer pair was run on the gels to ensure lack of contaminants in the sample.

Transient Transfection of TMEM16A in HEK-293 Cells

The 'a' variant of mouse TMEM16A (excluding Exon 0, which encodes for an additional 57 amino acids upstream of the sequence used) was kindly provided by Dr. Lily Y. Jan, Howard Hughes Medical Institute, University of California, San Francisco. The full sequence used in our study is shown in Figure 1. The full-length open reading frame was sub-cloned into pIRES-hrGFP-1a vector (Agilent Technologies, Santa Clara, CA). Two transfection methods were used during the course of this study. The first method involved transiently transfecting HEK-293 cells with 1-3 μ g of mTMEM16A in a T25 cell culture flask using a 1:3 ratio of the X-tremeGENE 9 DNA Transfection Reagent (Roche Applied Science, Indianapolis, IN). Patch clamp experiments were

carried out 48-72 hours post-transfection. In other experiments, cells grown at 80% confluency were transfected with 1.5 µg of plasmid DNA using the Lipofectamine 3000 Transfection Kit (Thermo Fisher Scientific, Waltham, MA) and OPTI-MEM (1X) (Thermo Fisher Scientific) in a 35 mm dish. Because of the high transfection efficiency of the latter protocol, electrophysiological experiments were carried out after only 24 hours post-transfection, and for a period not exceeding 48 hours after transfection.

Site-Directed Mutagenesis

For the TMEM16A mutants S528A and T622A, single-point mutations and amino acid insertions were performed using the QuikChange® II XL Site-Directed Mutagenesis Kit (Agilent Technologies, Santa Clara, CA). Mutagenic primers were designed against the putative CaMKII phosphorylation sites S528 and T622 of mouse TMEM16A replacing the serine residue with alanine leaving the flanking regions unmodified. Amplified products were purified using the QIAquick Gel Extraction kit (Qiagen Inc, Valencia, CA) and sequenced at the Nevada Genomic Center (Reno, NV) for verification. Thermal cycling parameters were set to conditions according to the manufacturers' instructions. In short this included an initial step at 95°C for 1 min, followed by 18 cycles of denaturation at 95°C for 50 s, annealing at 60°C for 50 s and extension at 68°C for 1 min/kb of plasmid length. The amplified products were treated with the *Dpn* I restriction enzyme (10 U/µl) for approximately 1 hour at 37°C to digest parental methylated and hemimethylated DNA. The *Dpn* I-treated DNA was transformed using XL10-Gold ultracompetent cells (Agilent Technologies) and optimized in NZY⁺ broth for 1 hour before plating the reaction on Ampicillin-treated agar plates. Agar plates were incubated for 12 hours at 37°C. For the T273A and S730A mutations, those

plasmids were generated by Mutagenex (Ohio State University, Columbus, OH), a company specialized in creating new plasmid constructs and mutations.

Whole-Cell Patch Clamp Electrophysiology

Ca²⁺-activated Cl⁻ currents resulting from transiently mouse TMEM16A transiently transfected mouse into HEK 293 cells were recorded using the conventional whole-cell configuration of the patch-clamp technique using an Axopatch 200A amplifier (Molecular Devices-Axon, Foster City, CA), Digidata 1440A acquisition system (Molecular Devices-Axon), and pCLAMP 10 software (Molecular Devices-Axon). To examine the effects of phosphorylation-induced rundown, I_{ClCa} were elicited by pipette solutions containing either 0 or 5 mM ATP. The composition of the intracellular pipette solution also contained 10 mM BAPTA as the Ca²⁺ buffer, and free [Ca²⁺] was set to 500 nM by the addition of 7.08 mM CaCl₂. Intracellular free [Ca²⁺] was calculated using the calcium chelator program Maxchelator (<http://www.stanford.edu/~cpatton/maxc.html>). To reduce contamination of I_{ClCa} from other types of currents in our recordings, CsCl and tetraethylammonium chloride (TEA) were added to the pipette solution and TEA was added to the K⁺-free external solution (see composition below). Series resistance compensation was performed in all experiments. Cells were continuously superfused in the recording chamber with the external solution at a flow rate of approximately 1 ml/min. All electrophysiological recordings were obtained at room temperature.

Experimental protocols

I_{ClCa} was evoked immediately upon rupture of the cell membrane and its voltage-dependent properties were monitored every 10 s by stepping from a holding potential (HP) of -50 mV to +90 mV for 1 s, followed by repolarization to -80 mV for 1 s. Current-voltage (I-V) relationships were constructed after 10-15 min of cell dialysis by stepping

in 10 mV increments from HP to test potentials between -100 mV and +140 mV for 1 s, each step followed by a 1 s repolarizing step to -80 mV. For I-V relationships, I_{Ca} was expressed as current density (pA/pF) by dividing the current amplitude measured at the end of each voltage clamp step by the cell capacitance. For all figure panels showing a time course of I_{Ca} changes, the late current measured at +90 mV was usually normalized to the amplitude of the initial current elicited at time = 0 (this is approximately 30 s after the membrane patch and measuring cell capacitance). After measuring cell capacitance, the constant step protocol described above was initiated to monitor the changes of I_{Ca} over a 10-15 min period of intracellular dialysis.

Solutions

The external solution used in all patch clamp experiments had the following composition (mM): 126 NaCl, 10 Hepes, 8.4 TEA, 20 glucose, 1.2 MgCl₂ and 1.8 CaCl₂. The pH was adjusted to 7.35 with NaOH. The internal pipette solution was composed of the following (mM): 20 TEA, 106 CsCl, 10 Hepes, 10 BAPTA, 7.08 CaCl₂, 0 or 5 ATP, 0.545 (0 ATP) or 3 (5 mM ATP) MgCl₂ and 0.2 guanosine-tri-phosphate. All enzymes and analytical grade reagents were purchased from Sigma-Aldrich, St. Louis, MO. Drugs and peptides were purchased from the following sources: Okadaic acid, KN-93 and Cantharidin, Sigma-Aldrich; Autocamtide-2-related inhibitory peptide (ARIP), Enzo Life Science, Farmingdale, NY.

Statistical Analysis

All pooled data are expressed as means with error bars representing the s.e.m. Raw data were imported into Excel and the means exported to OriginLab 9.3 software (OriginLab Corp. Northampton, MA, U.S.A.) for plotting and testing of statistical significance between groups. Statistical significance between means was determined

using paired or unpaired Student's t test when two groups were compared, or one-way ANOVA for multiple group comparisons and the Tukey *post-hoc* test to determine which groups are statistically significant from each other. $P < 0.05$ was considered to be statistically significant. All graphs and current traces were uploaded to CorelDraw 12 (Ottawa, Ontario, Canada) for final processing of the figures.

RESULTS

We transiently expressed the mouse TMEM16A isoform containing only the 'a' splice variant (see Fig. 1 for the complete amino acid sequence) in HEK-293 cells. A recent study by Paulino et al. (30) revealed a detailed structure of mouse TMEM16A using a Cryo-EM approach and proposed that the protein is composed of ten instead of eight transmembrane domains, which is consistent with that suggested for the fungal TMEM16 protein from *Nectria haematococca* (3). The clone used in our study comprises a 956 amino acid sequence that lacks the 57 amino acid segment recently reported by Mazzone *et al.* (28) (encoded by the so-called Exon 0), which is upstream of splice variant 'a'. Figure 1 also highlights the four putative CaMKII sites analyzed in our study (all Serine or Threonine positions are relative to the NCBI protein sequence NP_848757.4).

Figure 2A-a shows TMEM16A-mediated I_{ClCa} recorded at various times after seal rupture in a cell dialyzed with 500 nM free Ca^{2+} and 5 mM ATP. The currents were elicited by a repetitive voltage clamp protocol applied every 10 s (displayed below the current traces). A significant rundown was observed which reached a steady state within 5 to 10 min (Fig. 2A-b). In contrast, the experiment in Figure 2B shows that removal of ATP from the pipette solution led to an initial increase in I_{ClCa} , which

stabilized to a level that was higher than the initial current recorded immediately after breaking the seal. On average, TMEM16A-mediated I_{ClCa} decreased to $25.4 \pm 2.8\%$ (n=5) relative to the initial current recorded after seal rupture over the course of 17 minutes of cell dialysis in the presence of 5 mM ATP, whereas the current in cells lacking ATP displayed little rundown and stabilized to $113 \pm 16\%$ (n=9) relative to the initial current recorded at time = 0 (Fig. 3A and 3B)(0 ATP vs. 5 mM ATP, $P < 0.01$). Although TMEM16A-induced I_{ClCa} in HEK-293 cells ran down more slowly, these data display remarkable similarity with the behavior of native I_{ClCa} in rabbit pulmonary artery smooth muscle cells (PASMC)(1, 2, 47). TMEM16A currents were similar in magnitude at time = 0 ($P > 0.05$; Fig. 3C) but were more than 2-fold greater in magnitude in cells dialyzed with 0 ATP than those supplied with ATP after 20 min of cell dialysis, and displayed strong outwardly rectifying properties as previously reported for this channel when elicited by $[Ca^{2+}]_i < 1 \mu M$ (Fig. 3D). These results demonstrate that Cl^- currents produced by expression of TMEM16A displays ATP-dependent rundown that is similar to the phosphorylation-mediated regulation of CaCCs in vascular smooth muscle cells.

Rundown of TMEM16A-Induced I_{ClCa} is Attenuated by CaMKII Inhibition

Previous studies showed that calmodulin-dependent protein kinase II (CaMKII) mediated phosphorylation-induced rundown of I_{ClCa} in airway and arterial myocytes (13, 46). We next assessed whether the rundown of TMEM16A-induced I_{ClCa} observed in cells dialyzed with ATP was sensitive to CaMKII inhibition. We tested the contribution of CaMKII activity by dialyzing HEK-293 cells with the autocamtide-2-related inhibitory peptide (ARIP), a 13 amino acid synthetic peptide that is a potent and selective inhibitor of CaMKII (19). Application of 5 μM ARIP significantly attenuated the rundown seen in the presence of 5 mM ATP over the course of a 10 min period of cell dialysis (Fig. 4A; n

= 8). Enhancement of the TMEM16A-induced I_{ClCa} by the peptide inhibitor was also evident when comparing typical families of membrane currents recorded 10 min after cell rupture to determine the voltage-dependence of the currents with or without CaMKII inhibition (Fig. 4B-a). Figure 4B-b shows mean I-V curves for late currents (measured at the end of 1 s steps) registered with pipette solutions containing 5 mM ATP (n = 17), with (n=6) or without 5 μ M ARIP (n = 17). Similar to data obtained in the absence of drug, cells dialyzed with 5 μ M ARIP reversed near the predicted E_{Cl} (~ 0 mV) and displayed outward rectification at positive potentials. A marked enhancement of current density at both negative and positive potentials was clearly evident in ARIP-treated cells.

Intracellular application of KN-93 (10 μ M), another potent and highly selective inhibitor of CaMKII (IC_{50} = 0.37 μ M)(37) to HEK-293 cells overexpressing TMEM16A attenuated the rundown of I_{ClCa} to a level that was quantitatively similar to that produced by ARIP (Fig. 4C; ARIP: 0.679 ± 0.06 , n = 8; KN-93 0.625 ± 0.071 , n = 8; P = 0.562). While currents recorded in the absence of the drug ran down to approximately 33% of their initial amplitude, those from cells treated with KN-93 only decayed to approximately 63% of their initial level at the end of a 10 min period of cell dialysis (Control: 0.327 ± 0.03 , n = 23; KN-93: 0.625 ± 0.071 ; n = 8; p < 0.001). Taken together these data indicate that a significant portion of the rundown of TMEM16A-induced I_{ClCa} in cells supplied with intracellular ATP may involve at least one phosphorylation step mediated by CaMKII activity.

Effects of PP1/PP2A Inhibitors on TMEM16A-Induced I_{ClCa}

Studies in PSMCs revealed that both Ca^{2+} -dependent and Ca^{2+} -independent phosphatases augmented I_{ClCa} (2, 14). We therefore performed experiments to

ascertain if a similar regulation occurred for TMEM16A. We utilized okadaic acid (OA), a non-specific PP1/PP2A inhibitor, to determine whether TMEM16A-induced I_{ClCa} are modulated by the Ca^{2+} -independent serine/threonine protein phosphatases PP1 and PP2A. As shown in Figure 5A, an intracellular application of 30 nM OA, a concentration that would potentially block both PP1 and PP2A (6, 35), promoted significant rundown of TMEM16A-induced I_{ClCa} with normalized late I_{ClCa} stabilizing around 40% of the initial current (0 ATP: $113 \pm 16\%$, $n = 9$; 0 ATP + 30 nM OA: $42.9 \pm 11.8\%$, $n = 10$; $P < 0.001$), which was similar to the behavior of the current in cells intracellularly supplied with 5 mM ATP (Figs. 2 and 3). Analysis of the I-V relationships for late I_{ClCa} in the two conditions showed that OA inhibited TMEM16A current density by more than 50% at all test potentials (Fig. 5B). Use of Cantharidin (100 nM), another non-selective PP1/PP2A inhibitor, produced relatively similar effects on the time course of changes for I_{ClCa} during dialysis with no ATP when compared to cells treated with OA (data not shown; 0 ATP: $109 \pm 5.6\%$, $n=11$; 0 ATP + Cantharidin: $73.3 \pm 7.9\%$, $n=6$; $P < 0.001$). These data suggest that TMEM16A channels are modulated by PP1/PP2A in a manner that is remarkably similar to native I_{ClCa} in PSMCs (2).

Expression of CaMKII, PP1 and PP2A in HEK 293 cells

Using a rabbit anti-CaMKII pan antibody, we were able to successfully detect CaMKII in cultured HEK-293 cells (Fig. 6A). The cells displayed a fairly uniform expression of CaMKII within the cytosol. Immunocytochemical experiments were also performed to determine the endogenous expression of PP1 and PP2A. This was achieved by using isoform-specific antibodies for PP1 (PP1 α , PP1 β/δ , and PP1 γ) as well as a non-isoform specific antibody for PP2A. These experiments revealed fluorescent signals for PP2A as well as the three isoforms of PP1, all of which were

primarily localized in the cytosol (Fig. 6A). Additionally, CaMKII expression was also detected at the mRNA level. Using primers designed against non-conserved sequences of the CaMKII α , β , γ , and δ isoforms (see Table 1), we found that all four isoforms (and some alternatively spliced CaMKII α and γ transcripts) were expressed (Fig. 6B). Finally, Western blot experiments were also carried and confirmed the expression of several isoforms of the catalytic subunits of CaMKII (predicted molecular weights ranging from between ~ 50-70 kD, and single bands for all three isoforms of PP1 (predicted molecular weights between ~ 35 and 40 kD) and two isoforms of PP2A (predicted molecular weights between ~ 35 and 40 kD). These results confirmed the presence of CaMKII, PP1 and PP2A in the HEK-293 cell line used in our electrophysiological experiments.

Mutational Analysis of Potential TMEM16A Phosphorylation Sites by CaMKII

The data presented so far provide strong evidence that TMEM16A is regulated by kinase and phosphatase activity. Several putative serine/threonine phosphorylation sites have been predicted based on sequence analysis, including PKA, PKC, PKG, Casein kinase, and CaMKII (18, 21). By far the most common consensus sequences for phosphorylation by CaMKII are RXXT*/S* (21). We identified four such putative CaMKII phosphorylation sites (Fig. 7) on TMEM16A segments previously or currently believed to be located on the cytoplasmic side of the membrane (44, 50). Based on the original eight transmembrane TMEM16A protein model (5, 16, 34, 49), we had identified Threonine 622 as a potential consensus site for phosphorylation by CaMKII bearing the RXXT signature sequence. This residue was particularly appealing due to its apparent proximity to the pore-forming domain and recent evidence derived from the crystal structure of the fungal TMEM16 protein from *Nectria haematococca* (3). Experiments

with wild type TMEM16A and this mutant were performed on the same batch of cells, alternating between the two isoforms. TMEM16A bearing the T622A mutation displayed a nearly superimposable rundown relative to that of cells expressing wild type TMEM16A (data not shown; $P > 0.05$). Analysis of the voltage-dependence of maximal current after 5 min of cell dialysis with 5 mM ATP showed that the relationships were statistically superimposable, suggesting that T622 is not involved in the regulation of TMEM16A by CaMKII ($P > 0.05$). These results are consistent with the revised structure of TMEM16A where this residue is now thought to be embedded in transmembrane domain 4 of mouse TMEM16A (30).

We next sought to examine the other three CaMKII phosphorylation sites (T273, S528 and S730) now believed to lie on the cytoplasmic side of the protein by mutating each site to a neutral Alanine, one at a time. Figure 8A shows typical currents (normalized to an identical arbitrary scale) recorded at three different times following seal rupture for wild type TMEM16A, and TMEM16A carrying the T273A or S730A mutation. These experiments show that the current displayed very similar rundown over a 10 min time period. Figure 8B shows that the initial current amplitude at time = 0 of the S730A mutant was significantly smaller than that of wild type TMEM16A and the T273A mutant. A reduction in current density associated with this mutation is not an uncommon observation, even for single-point mutagenesis experiments. We can only speculate that the mutation may have altered transfection, transcription, translation and/or trafficking efficiency, which will require further investigation. The mean data for such experiments clearly demonstrate however that the ~ 70% rundown of TMEM16A-induced current was unaffected by mutating T273 or S730 to an Alanine, suggesting that either residue is not involved in the regulation of TMEM16A by CaMKII. Our data with S730A contrast

with those of Lin *et al.* (25) who showed that the corresponding residue (S727) of native TMEM16A in mouse basilar artery smooth muscle cells was the residue phosphorylated by CaMKII γ .

We next investigated the serine residue at position 528, which is located in the first intracellular loop of TMEM16A (Fig. 1). This amino acid is interesting because of its proximity to the peptide segments encoded by exons 13 (splice variant 'c') and 15 (splice variant 'd'), which have been shown to alter the Ca²⁺- and voltage-dependence, as well as activation and deactivation kinetics of TMEM16A-induced I_{ClCa} expressed in HEK-293 cells (10, 27, 48). We performed site-directed mutagenesis on this Serine again by replacing it with the nonpolar amino acid Alanine (S528A). In contrast to the other mutated residues, rundown of TMEM16A-induced I_{ClCa} was partially but significantly attenuated compared to wild type TMEM16A current in HEK-293 cells expressing the S528A mutant dialyzed with 5 mM ATP, an effect which was not affected by including KN-93 (10 μ M) in the pipette solution (Fig 9A). Late TMEM16A-induced current at +90 mV recorded from the S528A mutant, with or without KN-93, dialyzed with 5 mM ATP ran down to approximately 60% of the initial amplitude registered at $t = 0$, whereas currents recorded from wild type TMEM16A over-expressing cells displayed a more pronounced rundown with levels stabilizing to approximately 33% of the initial amplitude (S528A: 0.589 ± 0.087 , $n = 19$; S528A + KN-93: 0.602 ± 0.088 , $n=9$; WT: 0.327 ± 0.03 , $n = 23$; $P < 0.01$). These data suggest that Serine at position 528 may provide the necessary substrate for CaMKII leading to partial down-regulation of TMEM16A-induced I_{ClCa} by phosphorylation. Associated with the diminished rundown of TMEM16A-induced I_{ClCa} was the observation that outwardly rectifying I_{ClCa} measured at positive potentials for the S528A mutant was lower than the wild type TMEM16A-

induced current. The mean late I_{ClCa} for the S528A mutant dialyzed with 5 mM ATP for 10 min was 64.8 ± 10.5 pA pF⁻¹ at +120 mV (n = 8) compared to 200.8 ± 41.3 pApF⁻¹ (n = 14) for the wild type isoform (P < 0.05). This led us to examine whether the current density of I_{ClCa} for HEK-293 cells expressing this mutant was of lower magnitude than that of control cells immediately after seal rupture. We found that the current density recorded immediately upon membrane rupture ($t = 0$) was significantly reduced in the S528A mutants (118.8 ± 13.3 pA pF⁻¹) compared to current density of wild type TMEM16A (339.0 ± 37.2 pA pF⁻¹; P < 0.001; Fig. 9B, left panel). To determine whether this difference in current density was due to differences in voltage sensitivity we normalized the family of currents generated in wild type TMEM16A and S528A mutant expressing cells (both group of cells dialyzed with 5 mM ATP) to the maximal current recorded at +120 mV in their respective group. Analysis of the voltage-dependence of normalized current indicated that the voltage sensitivity was not significantly different between the two isoforms (Fig. 9B, right panel). These data show that similar to the S730A mutant, the current density of I_{ClCa} was significantly reduced in HEK-293 cells expressing TMEM16A S528A but this was not associated with a change in voltage sensitivity.

Cells expressing the S528A mutant displayed current rundown that was similar to the partial rundown observed for wild type TMEM16A current in the presence of either one of the two specific CaMKII inhibitors tested (Fig 4). To confirm this observation, we superimposed the mean time courses for S528A-induced currents with wild type TMEM16A-induced currents recorded in cells incubated with or without KN-93, or ARIP (Fig. 9C). Analysis of these results revealed that the rundown of TMEM16A-induced I_{ClCa} in the three conditions was not significantly different (One-Way ANOVA, P = 0.76).

Currents from S528A mutants were also recorded in the absence of ATP in order to minimize phosphorylation. When global phosphorylation was suppressed, rundown of I_{ClCa} from the S528A mutant was not significantly different from that of wild type TMEM16A also recorded in the absence of ATP (S528A: 0.842 ± 0.08 , $n = 21$, vs. WT: 1.038 ± 0.098 , $n = 13$; $P = 0.13$; Fig. 9D).

DISCUSSION

CaCC activity is suppressed in airway and vascular smooth muscle cells by mechanisms involving at least one phosphorylation step mediated, at least in part, by CaMKII (13, 22, 23, 46). In the present study, we sought to determine whether TMEM16A is regulated in a similar manner to native CaCCs. We show that currents resulting from expressing mouse TMEM16A in HEK-293 cells display remarkably similar properties to those of vascular myocytes: 1) TMEM16A-induced I_{ClCa} quickly runs down after seal rupture; 2) the rundown is largely prevented by omitting ATP from the pipette solution; 3) the rundown is partially prevented by inhibition of CaMKII; and 4) the up-regulation of TMEM16A seen in the absence of ATP is suppressed by inhibition of the Ca^{2+} -independent phosphatases PP1/PP2A. Moreover, our study identified a Serine residue (Serine 528) in the first intracellular loop of TMEM16A that is potentially involved in the phosphorylation of the anion channel by CaMKII.

Mouse TMEM16A Activity is Suppressed by CaMKII

Our study demonstrated that the Cl^- current produced by the expression of mouse TMEM16A “a” splice variant consistently ran down after seal rupture in HEK-293 cells supplied with 5 mM ATP and 500 nM free $[Ca^{2+}]_i$ to activate the channels. Although this phenomenon displayed a slightly slower time course and was less pronounced than that previously described by our group in rabbit PSMCs (Figs. 2 and 3)(1, 2, 14, 47),

the overall behavior was very similar with the anion current stabilizing to a new steady-state level within 5 to 10 min and remaining stable for more than 20 min.

The key observation that current rundown was abolished by removing ATP is reminiscent of that shown for I_{ClCa} in arterial myocytes (1, 2, 47). To our knowledge, only one other study reported a spontaneous decay of TMEM16A currents after membrane rupture in HEK-293 cells under whole-cell recording conditions similar to ours (43). In this report, the authors also showed that the rundown was potently inhibited by a 2h pre-incubation with the CaMKII inhibitor KN-62 (25 μ M) and was increased by the intracellular application of a Ca^{2+} -independent constitutive active form of CaMKII.

Application of two specific CaMKII inhibitors KN-93 (10 μ M) and ARIP (5 μ M) led to a significant but partial attenuation of the rundown of TMEM16A currents. These data also fall in line with previous studies indicating that CaMKII is involved in the regulation of I_{ClCa} in airway (46) and arterial myocytes (2, 13, 24). Immunocytochemical and Western blot experiments confirmed the presence of CaMKII at the protein level in HEK-293 cells, while RT-PCR studies identified transcripts for all four known isoforms (CaMKII α , CaMKII β , CaMKII γ and CaMKII δ), which indicates that this cell line was suitable for engaging in experiments evaluating the regulation of expressed TMEM16A by endogenous CaMKII. At the concentrations used, both inhibitors would be expected to exert maximal or near maximal inhibition of the enzyme (19, 37). Interestingly the magnitude of their effect on current decay was statistically indistinguishable. These results (along with our site-directed mutagenesis experiments discussed below) suggest that the latter experiments most likely revealed the full extent of the response and indicate that phosphorylation by CaMKII only partially (~40-50%) contributes to the

rundown of TMEM16A currents, suggesting the involvement of another mechanism also relying on intracellular ATP.

Regulation of TMEM16A-induced I_{ClCa} by Ca^{2+} -Independent Serine/Threonine Phosphatases

We used the specific PP1/PP2A inhibitor okadaic acid (OA) to determine whether TMEM16A-induced I_{ClCa} were regulated by the Ca^{2+} -independent serine/threonine protein phosphatases PP1 and PP2A. Intracellular application of OA (30 nM), a strategy previously used to examine the regulation of I_{ClCa} by these phosphatases in rabbit PSMCs (2), significantly attenuated TMEM16A-induced I_{ClCa} in HEK-293 cells dialyzed with no ATP. This time course is similar to the results obtained in rabbit PSMCs (2), which suggests that TMEM16A-mediated I_{ClCa} are similarly modulated by protein phosphatase activity. Another non-selective PP1/PP2A blocker, Cantharidin also promoted the rundown of TMEM16A-induced currents in cells dialyzed with no ATP and reduced TMEM16A channel conductance by approximately half. As for CaMKII, immunolabeling and Western blot experiments confirmed the presence of PP1 α , PP1 β , PP1 γ as well as PP2A in this cell line.

In contrast to our observations, Tian *et al.* (42) reported no effect of a 2h preincubation with 10 nM OA on expressed TMEM16A recorded under similar conditions with the exception that their pipette solution contained 3 mM ATP. We can only speculate that the inclusion of ATP promoted phosphorylation by CaMKII and perhaps other enzymes, which opposed the effects of phosphatases. Because TMEM16A-induced current (and native I_{ClCa} in PSMCs) always displays significant rundown in the presence of ATP, its regulation must be dominated by kinase activity,

which is most likely sufficiently potent to overwhelm phosphatase activity but answering this question will require more investigation.

Serine 528 Is a Target for CaMKII-Mediated Phosphorylation

Several putative serine/threonine phosphorylation sites were identified in mouse TMEM16A based on sequence analysis (18, 21). We initially identified three sites bearing the well-known consensus sequence “RXXS*/T*” for phosphorylation by CaMKII on the domains of TMEM16A predicted to lie on the cytoplasmic side of the membrane; this early assessment was based on the first model of this anion channel that predicted an eight transmembrane domain topology (5, 34, 44, 49, 50). Sequence analysis of the region surrounding these three sites (T273, S528 and T622) showed a high degree of homology between mouse, rat and human (Fig. 7B). The only difference is a conservative mutation of the arginine in mouse (and rat) at position 525 for a lysine at the –3 position in human (relative to the mouse sequence). The “KXXS*/T*” sequence has recently been documented to be a substrate for phosphorylation and regulation by CaMKII of the metabotropic glutamate receptor type Ia (20). The recent findings that the distant relative of TMEM16A in the fungus *Nectria haematococca* (3), and mouse TMEM16A (30), were both found to exhibit ten instead of eight transmembrane domains unraveled the existence of a new CaMKII phosphorylation site (S730) previously thought to lie outside the membrane but now localizing within the 3rd intracellular loop between TMD6 and TMD7 (Fig. 1). Notably, the region surrounding this potential site is not well conserved when rodent TMEM16A sequences are compared to the human sequence, which contains several non-conservative mutations (Fig. 7B).

Site-directed mutagenesis experiments were thus undertaken to identify the possible CaMKII phosphorylation site(s) involved in regulating TMEM16A. Mutating

Threonine at position 622 (now considered to lie within TMD4), or Serine residues at positions 273 (N-terminal domain) and 730 to a neutral Alanine, did not affect current rundown suggesting that these amino acids are not involved in the regulation of TMEM16A by CaMKII. In contrast, mutating the Serine at position 528 to an Alanine partially attenuated I_{ClCa} rundown; this reduction of rundown was unaffected by including the CaMKII inhibitor KN-93 in the pipette solution indicating that the significant effect of the latter (and likely ARIP) seen on wild type TMEM16A was not due to an off-target effect on another signaling pathway indirectly regulating TMEM16A. Interestingly, the time course and magnitude of I_{ClCa} rundown with this TMEM16A mutant was statistically indistinguishable to that exerted by two structurally unrelated CaMKII inhibitors on wild type TMEM16A, which supports the hypothesis that S528 is a major site targeted by CaMKII. This site also scored highest of the four (T273: 3.4; S528: 7.231; T622: not scored; S730: 3.82) based on bioinformatics analysis using Group-based Prediction System software (v. 3.0; source: <http://gps.biocuckoo.org>). In a recent study, Lin *et al.* (25) instead proposed that Serine 730 (Serine 727 in their case), but not S528 (S525 in their case), is the site phosphorylated by CaMKII γ in mouse basilar artery smooth muscle cells (BASMC). We can only speculate to the use of different cell types and experimental conditions to explain such differences. In their study, the investigators did not provide time courses of changes in the current after seal rupture so it is not possible to know if those recordings were obtained after membrane rupture or following a period of dialysis with elevated Ca^{2+} and ATP, and whether this impacted their results. In all our previous studies using vascular myocytes and in this study with expressed mouse TMEM16A, the regulation of this channel by intracellular ATP and enzymes took several minutes to develop after seal rupture. When dialyzed with 500 nM Ca^{2+} , native I_{ClCa} in

BASMCs or BASMCs transfected with an empty plasmid vector were extremely small or inexistent (25), which is at odd with other studies in mouse cerebral myocytes, which exhibited robust native *I_{Ca}* (4, 41). Although the results of Lin *et al.* (25) strongly supported the hypothesis that S730 is the residue involved in the regulation of TMEM16A by CaMKII, an unexplained finding from their study was the fact that transfection of BASMCs with TMEM16A carrying the phosphomimetic mutation S528 to Aspartate (S525D in their case) led to inhibited currents relative to those recorded from the expression of S528A. Clearly, additional experiments are required to clarify these apparent discrepancies.

In summary, data presented in this report show that overexpressed TMEM16A-induced *I_{Ca}* in HEK-293 cells display rundown and are regulated by CaMKII and PP1/PP2A in a manner that is similar to native *I_{Ca}* in rabbit PSMCs (2, 13, 14, 47). Our data also suggest that Serine 528 is an important contributor to the regulation of TMEM16A. It will be of great interest to assess the potential role of other splice variants in this process as the S528 is located between splice variants 'c' and 'd', both of which were shown to alter the voltage- and Ca²⁺-dependence, kinetics and pharmacology of TMEM16A (12, 27, 39, 48). Our results also suggest that another unidentified kinase(s) or mechanism(s) is involved in the regulation of TMEM16A because blocking CaMKII specifically or suppressing a potential phosphorylation site by a single-point mutation led to a similar partial attenuation of the rundown. This additional CaMKII-independent fraction of TMEM16A regulation was demonstrated by removing ATP from the pipette solution. Whether PIP₂ regulation of native CaCCs (32) and expressed TMEM16A (9, 40), or one or several other kinases, is involved in this process remains to be determined.

ACKNOWLEDGEMENTS

The authors would like to thank Talia Joyce for her technical support, and Dr. Lily Jan from the University of California, San Francisco, for gracefully providing us with the mouse TMEM16A clone.

GRANTS

This study was supported by grants to NL from the NIH (Grants R01 HL075477, R01 HL091238 and R01 HL146054) and the University of Nevada, Reno (VPRI REG 1200-121-1207), to IAG from the British Heart Foundation (PG/14/57/30992) and to CAS from the NIH (R01 HL127192). The publication was also made possible by a grant to NL (NCRR 5 P20 RR15581) from the National Center for Research Resources (NCRR), now part of the National Institute of General Medical Sciences, which supported a Center of Biomedical Research Excellence (COBRE) at the University of Nevada, Reno School of Medicine from 2000 to 2010. Confocal imaging experiments were supported by the High Spatial and Temporal Resolution Imaging Core of the new Center of Biomedical Research Excellence for Molecular and Cellular Signal Transduction in the Cardiovascular System funded by NIGMS grant 1P20GM130459 (NL). The contents of the manuscript are solely the responsibility of the authors and do not necessarily represent the official views of NCRR or NIH. RJA was supported by an NIH Ruth L. Kirschstein National Research Service Predoctoral Fellowship (F31 HL090023).

DISCLOSURES

No conflicts of interest, financial or otherwise, are declared by the authors.

References

1. **Angermann JE, Sanguinetti AR, Kenyon JL, Leblanc N, and Greenwood IA.** Mechanism of the inhibition of Ca^{2+} -activated Cl^- currents by phosphorylation in pulmonary arterial smooth muscle cells. *J Gen Physiol* 128: 73-87, 2006.
2. **Ayon R, Sones W, Forrest AS, Wiwchar M, Valencik ML, Sanguinetti AR, Perrino BA, Greenwood IA, and Leblanc N.** Complex phosphatase regulation of Ca^{2+} -activated Cl^- currents in pulmonary arterial smooth muscle cells. *J Biol Chem* 284: 32507-32521, 2009.
3. **Brunner JD, Lim NK, Schenck S, Duerst A, and Dutzler R.** X-ray structure of a calcium-activated TMEM16 lipid scramblase. *Nature* 516: 207-212, 2014.
4. **Bulley S, Neeb ZP, Burris SK, Bannister JP, Thomas-Gatewood CM, Jangsangthong W, and Jaggar JH.** TMEM16A Channels Contribute to the Myogenic Response in Cerebral Arteries. *Circ Res* 111: 1027-1036, 2012.
5. **Caputo A, Caci E, Ferrera L, Pedemonte N, Barsanti C, Sondo E, Pfeiffer U, Ravazzolo R, Zegarra-Moran O, and Galiotta LJ.** TMEM16A, a membrane protein associated with calcium-dependent chloride channel activity. *Science* 322: 590-594, 2008.
6. **Cohen P, Holmes CF, and Tsukitani Y.** Okadaic acid: a new probe for the study of cellular regulation. *Trends Biochem Sci* 15: 98-102, 1990.
7. **Davis AJ, Forrest AS, Jepps TA, Valencik ML, Wiwchar M, Singer CA, Sones WR, Greenwood IA, and Leblanc N.** Expression profile and protein translation of TMEM16A in murine smooth muscle. *Am J Physiol Cell Physiol* 299: C948-C959, 2010.
8. **Davis AJ, Shi J, Pritchard HA, Chadha PS, Leblanc N, Vasilikostas G, Yao Z, Verkman A, Albert AP, and Greenwood IA.** Potent vasorelaxant activity of the TMEM16A inhibitor T16A_{Inh}-A01. *Br J Pharmacol* 168: 773-784, 2013.
9. **De Jesus-Perez JJ, Cruz-Rangel S, Espino-Saldana AE, Martinez-Torres A, Qu Z, Hartzell HC, Corral-Fernandez NE, Perez-Cornejo P, and Arreola J.** Phosphatidylinositol 4,5-bisphosphate, cholesterol, and fatty acids modulate the calcium-activated chloride channel TMEM16A (ANO1). *Biochim Biophys Acta* 1863: 299-312, 2018.
10. **Ferrera L, Caputo A, Uby I, Bussani E, Zegarra-Moran O, Ravazzolo R, Pagani F, and Galiotta LJ.** Regulation of TMEM16A chloride channel properties by alternative splicing. *J Biol Chem* 284: 33360-33368, 2009.
11. **Forrest AS, Joyce TC, Huebner ML, Ayon RJ, Wiwchar M, Joyce J, Freitas N, Davis AJ, Ye L, Duan DD, Singer CA, Valencik ML, Greenwood IA, and Leblanc N.** Increased TMEM16A-encoded calcium-activated chloride channel activity is associated with pulmonary hypertension. *Am J Physiol Cell Physiol* 303: C1229-C1243, 2012.
12. **Galiotta LJ.** The TMEM16 protein family: a new class of chloride channels? *Biophys J* 97: 3047-3053, 2009.

13. **Greenwood IA, Ledoux J, and Leblanc N.** Differential regulation of Ca^{2+} -activated Cl^- currents in rabbit arterial and portal vein smooth muscle cells by Ca^{2+} -calmodulin-dependent kinase. *J Physiol* 534: 395-408, 2001.
14. **Greenwood IA, Ledoux J, Sanguinetti A, Perrino BA, and Leblanc N.** Calcineurin A α but not A β augments $\text{I}_{\text{Cl}(\text{Ca})}$ in rabbit pulmonary artery smooth muscle cells. *J Biol Chem* 279: 38830-38837, 2004.
15. **Hartzell C, Putzier I, and Arreola J.** Calcium-activated chloride channels. *Annu Rev Physiol* 67: 719-758, 2005.
16. **Hartzell HC, Yu K, Xiao Q, Chien LT, and Qu Z.** Anoctamin/TMEM16 family members are Ca^{2+} -activated Cl^- channels. *J Physiol* 587: 2127-2139, 2009.
17. **Heinze C, Seniuk A, Sokolov MV, Huebner AK, Klementowicz AE, Szijarto IA, Schleifenbaum J, Vitzthum H, Gollasch M, Ehmke H, Schroeder BC, and Hubner CA.** Disruption of vascular Ca^{2+} -activated chloride currents lowers blood pressure. *J Clin Invest* 124: 675-686, 2014.
18. **Huang RY, Laing JG, Kanter EM, Berthoud VM, Bao M, Rohrs HW, Townsend RR, and Yamada KA.** Identification of CaMKII phosphorylation sites in Connexin43 by high-resolution mass spectrometry. *J Proteome Res* 10: 1098-1109, 2011.
19. **Ishida A, Kameshita I, Okuno S, Kitani T, and Fujisawa H.** A novel highly specific and potent inhibitor of calmodulin-dependent protein kinase II. *Biochem Biophys Res Commun* 212: 806-812, 1995.
20. **Jin DZ, Guo ML, Xue B, Fibuch EE, Choe ES, Mao LM, and Wang JQ.** Phosphorylation and feedback regulation of metabotropic glutamate receptor 1 by calcium/calmodulin-dependent protein kinase II. *J Neurosci* 33: 3402-3412, 2013.
21. **Kennelly PJ, and Krebs EG.** Consensus sequences as substrate specificity determinants for protein kinases and protein phosphatases. *J Biol Chem* 266: 15555-15558, 1991.
22. **Leblanc N, Forrest AS, Ayon RJ, Wiwchar M, Angermann JE, Pritchard HA, Singer CA, Valencik ML, Britton F, and Greenwood IA.** Molecular and functional significance of Ca^{2+} -activated Cl^- channels in pulmonary arterial smooth muscle. *Pulm Circ* 5: 244-268, 2015.
23. **Leblanc N, Ledoux J, Saleh S, Sanguinetti A, Angermann J, O'Driscoll K, Britton F, Perrino BA, and Greenwood IA.** Regulation of calcium-activated chloride channels in smooth muscle cells: a complex picture is emerging. *Can J Physiol Pharmacol* 83: 541-556, 2005.
24. **Ledoux J, Greenwood I, Villeneuve LR, and Leblanc N.** Modulation of Ca^{2+} -dependent Cl^- channels by calcineurin in rabbit coronary arterial myocytes. *J Physiol* 552: 701-714, 2003.
25. **Lin CX, Lv XF, Yuan F, Li XY, Ma MM, Liu CZ, Zhou JG, Wang GL, and Guan YY.** Ca^{2+} /Calmodulin-Dependent Protein Kinase II gamma-Dependent Serine727 Phosphorylation Is Required for TMEM16A Ca^{2+} -Activated Cl^- Channel Regulation in Cerebrovascular Cells. *Circ J* 82: 903-+, 2018.

26. **Manoury B, Tamuleviciute A, and Tamaro P.** TMEM16A/Anoctamin1 protein mediates calcium-activated chloride currents in pulmonary arterial smooth muscle cells. *J Physiol* 588: 2305-2314, 2010.
27. **Mazzone A, Bernard CE, Strege PR, Beyder A, Galiotta LJ, Pasricha PJ, Rae JL, Parkman HP, Linden DR, Szurszewski JH, Ordog T, Gibbons SJ, and Farrugia G.** Altered expression of Ano1 variants in human diabetic gastroparesis. *J Biol Chem* 286: 13393-13403, 2011.
28. **Mazzone A, Gibbons SJ, Bernard CE, Nowsheen S, Middha S, Almada LL, Ordog T, Kendrick ML, Reid Lombardo K, Shen KR, Galiotta LJ, Fernandez-Zapico ME, and Farrugia G.** Identification and characterization of a novel promoter for the human ANO1 gene regulated by the transcription factor signal transducer and activator of transcription 6 (STAT6). *FASEB J* 29: 152-163, 2015.
29. **Morris AP, and Frizzell RA.** Ca²⁺-dependent Cl⁻ channels in undifferentiated human colonic cells (HT-29). 2. Regulation and rundown. *Am J Physiol Cell Physiol* 264: C977-C985, 1993.
30. **Paulino C, Kalienkova V, Lam AKM, Neldner Y, and Dutzler R.** Activation mechanism of the calcium-activated chloride channel TMEM16A revealed by cryo-EM. *Nature* 552: 421-425, 2017.
31. **Pedemonte N, and Galiotta LJ.** Structure and function of TMEM16 proteins (anoctamins). *Physiol Rev* 94: 419-459, 2014.
32. **Pritchard HA, Leblanc N, Albert AP, and Greenwood IA.** Inhibitory role of phosphatidylinositol 4,5 biphosphate on TMEM16A encoded calcium-activated chloride channels in rat pulmonary artery. *Br J Pharmacol* 171: 4311-4321, 2014.
33. **Reisert J, Bauer PJ, Yau KW, and Frings S.** The Ca-activated Cl channel and its control in rat olfactory receptor neurons. *J Gen Physiol* 122: 349-363, 2003.
34. **Schroeder BC, Cheng T, Jan YN, and Jan LY.** Expression cloning of TMEM16A as a calcium-activated chloride channel subunit. *Cell* 134: 1019-1029, 2008.
35. **Sheppeck JE, 2nd, Gauss CM, and Chamberlin AR.** Inhibition of the Ser-Thr phosphatases PP1 and PP2A by naturally occurring toxins. *Bioorg Med Chem* 5: 1739-1750, 1997.
36. **Simon Bulley SB, and Jaggar JH.** Cl⁻ channels in smooth muscle cells. *Pflugers Arch* 466: 861-872, 2014.
37. **Sumi M, Kiuchi K, Ishikawa T, Ishii A, Hagiwara M, Nagatsu T, and Hidaka H.** The newly synthesized selective Ca²⁺/calmodulin dependent protein kinase II inhibitor KN-93 reduces dopamine contents in PC12h cells. *Biochem Biophys Res Commun* 181: 968-975, 1991.
38. **Sun H, Xia Y, Paudel O, Yang XR, and Sham JS.** Chronic hypoxia-induced upregulation of Ca²⁺-activated Cl⁻ channel in pulmonary arterial myocytes: a mechanism contributing to enhanced vasoreactivity. *J Physiol* 590: 3507-3521, 2012.
39. **Sung TS, O'Driscoll K, Zheng H, Yapp NJ, Leblanc N, Koh SD, and Sanders KM.** Influence of intracellular Ca²⁺ and alternative splicing on the pharmacological profile of ANO1 channels. *Am J Physiol Cell Physiol* 311: C437-C451, 2016.

40. **Ta CM, Acheson KE, Rorsman NJG, Jongkind RC, and Tammaro P.** Contrasting effects of phosphatidylinositol 4,5-bisphosphate on cloned TMEM16A and TMEM16B channels. *Br J Pharmacol* 174: 2984-2999, 2017.
41. **Thomas-Gatewood C, Neeb ZP, Bulley S, Adebisi A, Bannister JP, Leo MD, and Jaggar JH.** TMEM16A channels generate Ca^{2+} -activated Cl^- currents in cerebral artery smooth muscle cells. *Am J Physiol Heart Circ Physiol* 301: H1819-H1827, 2011.
42. **Tian Y, Kongsuphol P, Hug M, Ousingsawat J, Witzgall R, Schreiber R, and Kunzelmann K.** Calmodulin-dependent activation of the epithelial calcium-dependent chloride channel TMEM16A. *FASEB J* 25: 1058-1068, 2011.
43. **Tian Y, Schreiber R, and Kunzelmann K.** Anoctamins are a family of Ca^{2+} -activated Cl^- channels. *J Cell Sci* 125: 4991-4998, 2012.
44. **Tien J, Peters CJ, Wong XM, Cheng T, Jan YN, Jan LY, and Yang H.** A comprehensive search for calcium binding sites critical for TMEM16A calcium-activated chloride channel activity. *eLife* 3: 2014.
45. **Wang M, Yang H, Zheng LY, Zhang Z, Tang YB, Wang GL, Du YH, Lv XF, Liu J, Zhou JG, and Guan YY.** Downregulation of TMEM16A calcium-activated chloride channel contributes to cerebrovascular remodeling during hypertension through promoting basilar smooth muscle cell proliferation. *Circulation* 125: 697-707, 2012.
46. **Wang YX, and Kotlikoff MI.** Inactivation of calcium-activated chloride channels in smooth muscle by calcium/calmodulin-dependent protein kinase. *Proc Natl Acad Sci U S A* 94: 14918-14923, 1997.
47. **Wiwchar M, Ayon R, Greenwood IA, and Leblanc N.** Phosphorylation alters the pharmacology of Ca^{2+} -activated Cl^- channels in rabbit pulmonary arterial smooth muscle cells. *Br J Pharmacol* 158: 1356-1365, 2009.
48. **Xiao Q, Yu K, Perez-Cornejo P, Cui Y, Arreola J, and Hartzell HC.** Voltage- and calcium-dependent gating of TMEM16A/Ano1 chloride channels are physically coupled by the first intracellular loop. *Proc Natl Acad Sci U S A* 108: 8891-8896, 2011.
49. **Yang YD, Cho H, Koo JY, Tak MH, Cho Y, Shim WS, Park SP, Lee J, Lee B, Kim BM, Raouf R, Shin YK, and Oh U.** TMEM16A confers receptor-activated calcium-dependent chloride conductance. *Nature* 455: 1210-1215, 2008.
50. **Yu K, Duran C, Qu Z, Cui YY, and Hartzell HC.** Explaining calcium-dependent gating of anoctamin-1 chloride channels requires a revised topology. *Circ Res* 110: 990-999, 2012.

FIGURE LEGENDS

Figure 1: Mouse Anoctamin-1 sequence used in our study (TMEM16A-a) with the position of the four predicted CaMKII sites (RXXT/S). The mouse clone used in our study only included splice variant 'a'. The position of the four hypothetical CaMKII phosphorylation sites shown in white font over a red background are relative to the NCBI protein database sequence NP_848757.4. Intracellular and extracellular domains are respectively shown in blue and black fonts. Transmembrane domains are labeled with underlined green fonts. The sequence of splice variant 'a' is shown in black font over a yellow background. TMDX: Transmembrane Domain X. The position of the transmembrane domains is based on the recent Cryo-EM study by Paulino et al. (30) revealing the quaternary structure of mouse TMEM16A.

Figure 2. Ca^{2+} -activated Cl^- currents elicited by mouse TMEM16A expression in HEK-293 cells run down in the presence of intracellular ATP. **(A)** Typical experiment illustrating the rundown of TMEM16A-induced I_{ClCa} in a HEK-293 cell dialyzed with 5 mM ATP and 500 nM free Ca^{2+} . Panel A-a shows superimposed current traces (top) recorded at selected times shown to the right of each trace. The currents were elicited by the voltage clamp protocol depicted below the traces and applied to the cell at a frequency of one step every 10 s. Panel A-b shows a plot of the time course of changes of the current measured at the end of the pulse to +90 mV for the experiment in panel A-a. Open circles report measurements for the traces depicted in panel A-a. **(B)** This panel shows a similar experiment carried out in a different cell dialyzed with 0 mM ATP and 500 nM free Ca^{2+} . The nomenclature for both panels is identical to that of panel A.

Figure 3. ATP-Dependence of TMEM16A-mediated I_{ClCa} and comparison with native I_{ClCa} . **(A)** Mean time courses of changes of normalized TMEM16A-induced I_{ClCa} measured at +90 mV in HEK-293 cells dialyzed with 0 (open circles; n=14) or 5 mM ATP (filled circles; n=26). Arrow indicates when current density was measured to compare the magnitude of the initial I_{ClCa} recorded at time = 0 in cells dialyzed with 0 or 5 mM ATP, for which mean data are reported in panel C. **(B)** Mean time courses of changes of native I_{ClCa} recorded in rabbit pulmonary artery smooth muscle cells (PASMCs) dialyzed with 0 (dashed line) or 5 mM ATP (solid line). The plot was adapted from research originally published by our group in The Journal of Biological Chemistry (Figure 3A-a). Ayon, R., Sones, W., Forrest, A. S., Wiwchar, M., Valencik, M. L., Sanguinetti, A. R., Perrino, B. A., Greenwood, I. A. and Leblanc, N.. *Journal of Biological Chemistry*. 2009; 284: 32507-32521. © The American Society for Biochemistry and Molecular Biology. Panels A and B emphasize the remarkable similarity in the response of TMEM16A and native I_{ClCa} to intracellular ATP. **(C)** Mean bar graph showing the magnitude of the initial late TMEM16A current (in pA/pF) recorded immediately after seal rupture ($t=0$) in cells dialyzed with 5 (black bar; n=23) or 0 mM (white bar; n=14) ATP. **(D)** Mean current-voltage (I-V) relationships for TMEM16A-induced I_{ClCa} recorded 20 min after seal rupture in HEK-293 cells dialyzed with 0 (open circles; n=15) and 5 mM ATP (filled circles; n=17). Both I-Vs displayed pronounced outward rectification and reversed around 0 mV, which is near the predicted equilibrium potential for Cl^- (E_{Cl}) in our conditions. For all panels: † P < 0.01; ‡ P < 0.001; n.s.: not significant.

Figure 4. Two structurally unrelated specific CaMKII inhibitors similarly attenuated the rundown of TMEM16A-induced I_{ClCa} . **(A)** Intracellular application of autocamtide-2-

related inhibitory peptide (ARIP; 5 μ M) significantly reduced the rundown of TMEM16A-induced I_{ClCa} in myocytes dialyzed with 5 mM ATP. Graph shows the mean time course of changes for TMEM16A-induced I_{ClCa} in HEK-293 cells dialyzed over 10 min with 5 mM ATP in the presence (open circles; n = 8) or absence of ARIP (filled circles, n = 23). **(B)** Panel B-a shows representative families of currents recorded from cells dialyzed with 5 mM ATP (upper traces), or 5 mM ATP + 5 μ M ARIP (lower traces). Panel B-b shows mean I-V curves generated from families of currents evoked by intracellular pipette solutions containing 5 mM ATP (n = 17) or 5 mM ATP plus 5 μ M ARIP (n = 6). Similar to control, cells dialyzed with 5 μ M ARIP reversed near E_{Cl} and displayed outward rectification at positive potentials. However, TMEM16A currents measured in cells treated with ARIP were significantly larger than those recorded in the absence of the inhibitor. **(C)** Graph shows the mean time courses of changes of normalized TMEM16A-generated I_{ClCa} for control cells dialyzed with 5 mM ATP (black squares, n = 23) and cells dialyzed with 5 mM ATP + 10 μ M KN-93 (red circles, n = 8). As for ARIP, KN-93 significantly mitigated the rundown seen in control cells dialyzed with 5 mM ATP alone. For all panels: * P < 0.05; † P < 0.01; ‡ P < 0.001.

Figure 5. *Modulation of TMEM16A-mediated I_{ClCa} by Ca^{2+} -independent serine/threonine protein phosphatase activity.* **(A)** This panel shows a plot of averaged time courses of changes of normalized TMEM16A-induced I_{ClCa} in HEK-293 cells dialyzed with 0 ATP, with (filled squares) or without (open circles) 30 nM okadaic acid (OA), a non-selective inhibitor of PP1 and PP2A. The graph shows that in the absence of ATP, TMEM16A-mediated I_{ClCa} displayed a small but significant transient rundown followed by a delayed recovery current recovery phase after ~ 9 min. **(B)** Mean I-V curves generated from families of currents evoked by intracellular pipette solutions containing 0 mM ATP (open circles; n = 14), or 0 mM ATP plus 30 nM OA (filled squares; n = 9), both after 20 min of cell dialysis. For all panels: * P < 0.05; † P < 0.01; ‡ P < 0.001.

Figure 6. *Endogenous expression of CaMKII and the Ca^{2+} -independent protein phosphatases PP1 and PP2A in non-transfected HEK-293 cells.* **(A)** Immunocytochemical detection of CaMKII (top left image) and PP2A (top middle image) protein expression was respectively performed using a primary rabbit polyclonal antibody against CaMKII from Santa Cruz Biotechnology (Dallas, TX; sc-9035) and a rabbit monoclonal antibody against the catalytic subunit of PP2A from Cell Signaling Technology (Danvers, MA; 52F8). Detection of both enzymes was carried out by incubating cells with a secondary anti-rabbit IgG Alexa Fluor[®] 546 (Thermo Fisher Scientific, Waltham, MA; A-11010). Cells serving as negative controls were incubated with the secondary antibody only (2nd Only; top right image). Immunocytochemical studies were also carried out to determine the endogenous expression of the catalytic subunits of PP1 α (bottom left upper image), PP1 β (bottom right upper image), and PP1 γ (bottom left lower image) in cultured HEK-293 cells. All antibodies were goat antibodies from Santa Cruz Biotechnology (PP1 α : sc-6105; PP1 β : sc-6107; PP1 γ : sc-6109). All cells were incubated with the goat anti-rabbit IgG Alexa Fluor[®] 488 (Thermo Fisher Scientific; A-11008) secondary antibody. Negative controls were labeled with secondary antibody only (2nd Only; bottom right lower image). A 60X oil immersion objective was used for detection of all enzymes. For all images in panel A, nuclei were stained with 4',6-diamidino-2-phenylindole (DAPI; (Abcam, Cambridge, UK). **(B)** Expression of CaMKII isoforms at the mRNA level was determined using specific primers designed against each of the four CaMKII isoforms (see Table 1). For each set

of primers pairs, a non-template control (NTC) was performed; however, for the sake of space, this figure shows a single representative NTC. PCR amplified products were resolved on a 2% agarose gel. Single bands for the CaMKII β and δ isoforms were detected in HEK-293 cells, which fall within the expected amplicon size (396 bp for both) based on primer design. Multiple bands were detected in HEK-293 cells for CaMKII α and γ , which is most likely the result of alternative splicing. Predicted amplicon size for CaMKII α : 452 bp; CaMKII γ : 413 bp. **(C)** Western blot analysis of non-transfected HEK-293 cells demonstrated the expression of several isoforms of CaMKII, all three known catalytic PP1 isoforms, and two isoforms of the catalytic subunit of PP2A. Proteins of interest and ladder appear in red while the housekeeping proteins GAPDH and β -Actin appear in green. 20 μ g of lysate protein were loaded in each lane.

Figure 7. *Proposed membrane topology and location of the four putative CaMKII phosphorylation sites identified on mouse TMEM16A.* **(A)** Proposed secondary structure of mouse TMEM16A highlighting the alternatively spliced variant 'a' located in the N terminus (thick green solid line), and approximate location of the proposed binding sites for Ca^{2+} based on the structure proposed by Paulino et al. (30), and the position of the four consensus sites for phosphorylation by CaMKII that obey the basic sequence RXXS/T (T273, S528, T561 and S730 all labeled with red circles). **(B)** Sequence homology between mouse, rat and human TMEM16A in the region surrounding each of the four identified potential CaMKII phosphorylation targets. The putative CaMKII RXXT/S sequence, and conservative and non-conservative amino acid replacements are highlighted in white font over a red, green or black background, respectively, as shown above the sequences. The amino acids highlighted in blue for the human sequence corresponds to splice variant 'd', which is not present in the mouse and rat sequences defined by the two NCBI protein accession numbers. However, the human sequence downstream of splice variant 'd' (not shown) defined by accession number NP_060513.5 is identical to the remaining sequence shown for mouse and rat (TDKVKLTWR).

Figure 8. *Substitution of Threonine 273 or Serine 528 to a neutral Alanine had no impact on the regulation of TMEM16A-Induced I_{ClCa} .* **(A)** Representative current traces recorded immediately ($t = 0 \text{ min}$), and after 2 ($t = 2 \text{ min}$) and 10 min ($t = 10 \text{ min}$) following membrane rupture demonstrating the time-dependent rundown of I_{ClCa} recorded from HEK-293 cells overexpressed with wild type TMEM16A (TMEM16A WT; top left), the T273A (TMEM16A T273A; top right) or the S730A mutant (TMEM16A S730A; bottom left), all recorded in the presence of 5 mM ATP in the pipette solution. The currents were evoked by 1 s steps to +90 mV from a holding potential of -50 mV; the inward tail current was elicited by a 1 s return step to -80 mV (bottom right). **(B)** Mean bar graph showing the amplitude of the initial current recorded at +90 mV at time = 0 from a holding potential of -50 mV (protocol identical to that shown in panel A, bottom right). Each bar is a mean \pm s.e.m. current density in pA/pF. **(C)** Graph showing the mean time courses of changes of normalized late I_{ClCa} elicited by depolarizing steps to +90 mV applied at a frequency of 0.1 Hz for WT TMEM16A (black circles), and the T273A (open squares) and S730A (open circles) mutants. Each data point is a mean \pm s.e.m. Mutation of the Threonine at position 273 or Serine at position 730 to an Alanine did not alter the time course and magnitude of TMEM16A-mediated I_{ClCa} rundown. n: number of cells. For panels B and C: n.s.: not significant; *: $P < 0.05$; ††: $P < 0.001$.

Figure 9. Mutation of Serine 528 to Alanine attenuates TMEM16A rundown to a level that is quantitatively similar to that exerted by specific CaMKII inhibitors. **(A)** Graph showing the mean time courses of changes of normalized late I_{Ca} elicited by depolarizing steps to +90 mV applied at a frequency of 0.1 Hz from holding potential of -50 mV for WT TMEM16A (black circles), or TMEM16A S528A mutant in the absence (open circles) or presence of 10 μ M KN-93 in the pipette solution (open squares). All currents were normalized to the initial current recorded immediately upon cell membrane rupture. The S528A mutation significantly reduced the rundown of TMEM16A-induced I_{Ca} HEK-293 cells over the course of a 10 min period of cell dialysis with 5 mM ATP (S528A: 0.589 ± 0.087 , $n = 19$; S528A + KN-93: 0.602 ± 0.088 , $n=9$; WT: 0.327 ± 0.030 , $n = 23$; $P < 0.01$). **(B) Left panel:** Mean bar graph showing the magnitude of the initial late TMEM16A current density \pm s.e.m. (in pA/pF) recorded after seal rupture ($t=0$) in cells dialyzed with 5 mM ATP for wild type TMEM16A (black bar; $n=14$) and the S528A mutant (white bar; $n=8$). **Right panel:** Mean I-V relationships for late I_{Ca} recorded from wild type TMEM16A (black circles) and the S528A mutant after seal rupture ($t=0$). Currents in each group were normalized to that recorded at +120 mV in their respective group. Data points in each group are means \pm s.e.m. **(C)** The time course plots shown in Fig. 4A and 4C were superimposed to those of panel A to illustrate the similarity between the attenuation of rundown of TMEM16A produced by the S528A mutation and that elicited by the two CaMKII inhibitors ARIP and KN-93. One-way ANOVA analysis revealed no significant difference between the three groups of data after 10 min of cell dialysis with 5 mM ATP ($P > 0.05$). **(D)** Graph showing the mean time courses of changes of normalized late I_{Ca} elicited by depolarizing steps to +90 mV applied at a frequency of 0.1 Hz from holding potential of -50 mV for WT TMEM16A (black triangles) or TMEM16A S528A mutant (open triangles) dialyzed with 0 ATP. The TMEM16A S528A mutant decayed over a 10 min period to a level that was approximately 16% of the initial amplitude, which was not significantly different from WT TMEM16A currents (1.038 ± 0.098 , $n = 13$; $P = 0.13$). For all panels: $\dagger\dagger P < 0.001$; $\dagger P < 0.01$; n.s.: not significant.

Table 1. *Primer Sequences for Detection of CaMKII, PP1 and PP2A Transcripts*

Gene	Primer Sequence F – Forward R – Reverse	GenBank Accession Number	Amplicon (bp)	Region Spanned
CaMKII α	F: 5'-TCCACCGTGGCATCCTGCAT-3' R: 5'-ATGGTGGTGTGCACGGGCTT-3'	NM_015981.3	452	1038-1489
CaMKII β	F: 5'-TGCATCCTCCTGCCAACGCA-3' R: 5'-TCGGCGAGAGGCCCAAAC-3'	NM_001220.4	396	2654-3049
CaMKII γ	F: 5'-AAGCGCATCACGGCTGACCA-3' R: 5'-ACCGAGCTGCCATTCCCAGT-3'	NM_172171.2	413	905-1317
CaMKII δ	F: 5'-TCGCAACTGCTTGCCACTCGT-3' R: 5'-TGTGGTCGAAGCCATCCTCGGT-3'	NM_172127.2	396	479-874

Mouse TMEM16A-a

INTRACELLULAR DOMAIN — EXTRACELLULAR DOMAIN — TRANSMEMBRANE DOMAIN**Variant a** (Excludes a 57 amino acid sequence encoded by Exon 0, which is upstream of the one shown below)

MRVPEKYSTLPAEDRSVHIVNICAIEDLGYPSEGTLNLSVDPDAECKYGLYFRDGRKRVYILVYHH

KRASGSRTLARRGLQNDMVLGTRSQRDQPLPGKGS PVDAGSPEVPMDYHEDDKRFRREEYEGNLLLEAGL

ELENDKTKIHGVGFKIHAPWHVLCREAEFLKLMPTKKVYHISETRGLLKTINSVLQKITDPIQPKVA

CaMKII (T273)

EHRPQT TKRLSYPF SREKQHLFDLTD RDSFFDSKTRSTIVYEILKRTTCTKAKYSMGITSLLANGVYSAA

TMD1

YPLHDGDYEGDNVEFNDRKLLYE EWASYGVFYKYQPIDLVRKYFG EKVGLYFAWL GAYTOMLIPASIVGV

TMD2

IVFLYGCATVDENIPSMEMCDQRYNITMCPLCDKTC SYWKMS SACATARASHLFDN PATVFFSVFMALWA**CaMKII (S528)**ATFMEHWKRKQMLNRYRDLTGFEEDHPRAEYEARVLEKSL RKES RNKETDKVKLTWRDRFPAYFTNL

TMD3

TMD4

VSIIFMIAVTFAIVLGVIIYRISTAAALAMNSSPSVRSNI RVTVTATAVIINLVVILLDEVYGCIA RWL**CaMKII (T622)**

TMD5

TKIEVPKTEKSFEERLTFKAFLLKFNSYTPIFYVAFFKGRFVGRPGDYVYIFRSFRMEECAPGGCLMEL

TMD6

CaMKII (S730)CIOLSIIMLGKOLIQNNLFEIGIPKMKKFIRYLKL RRQS PSDREEYVKKRQRYEVDFNLEPFAGLTPEYM

TMD7

TMD8

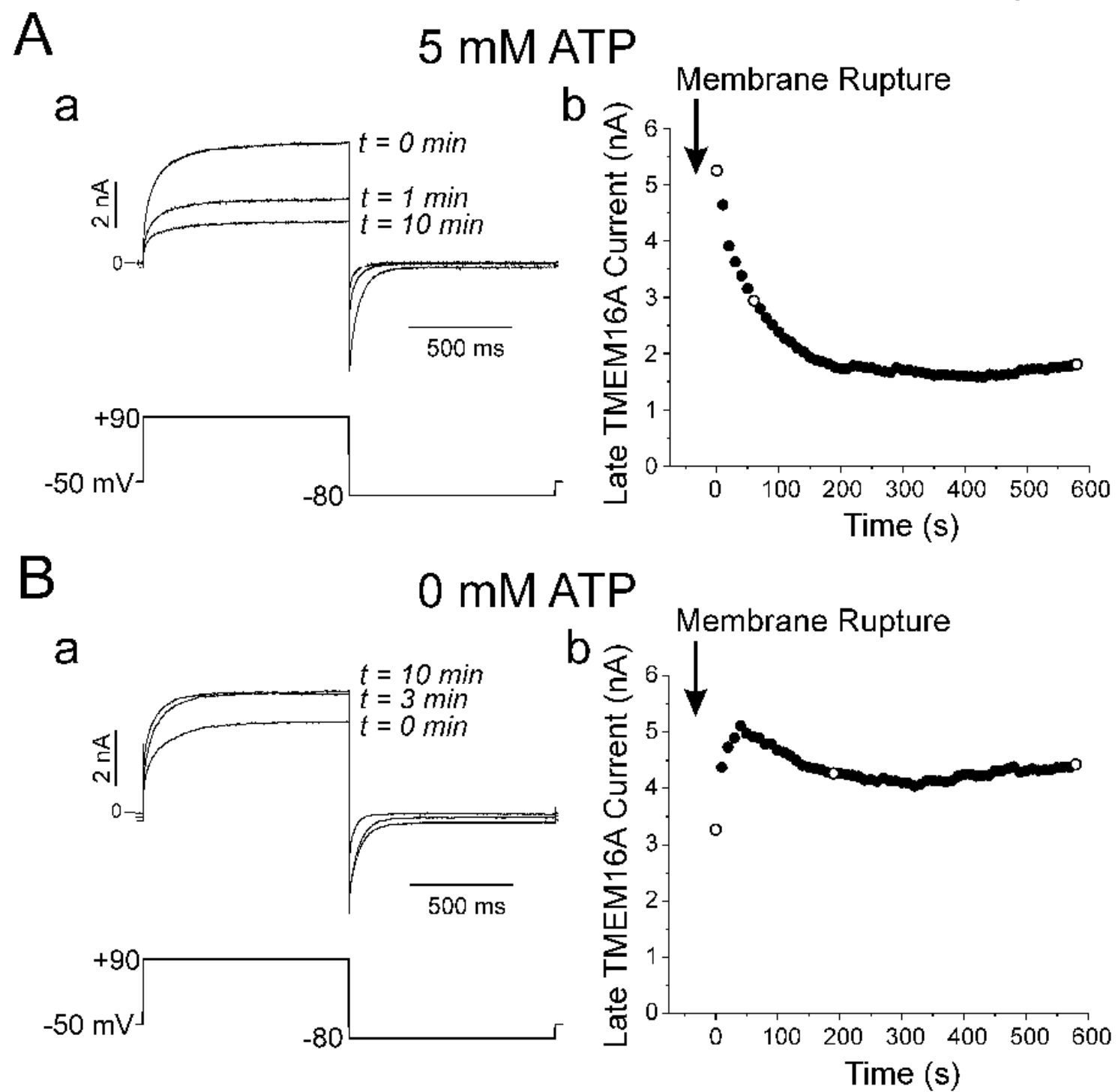
TMD9

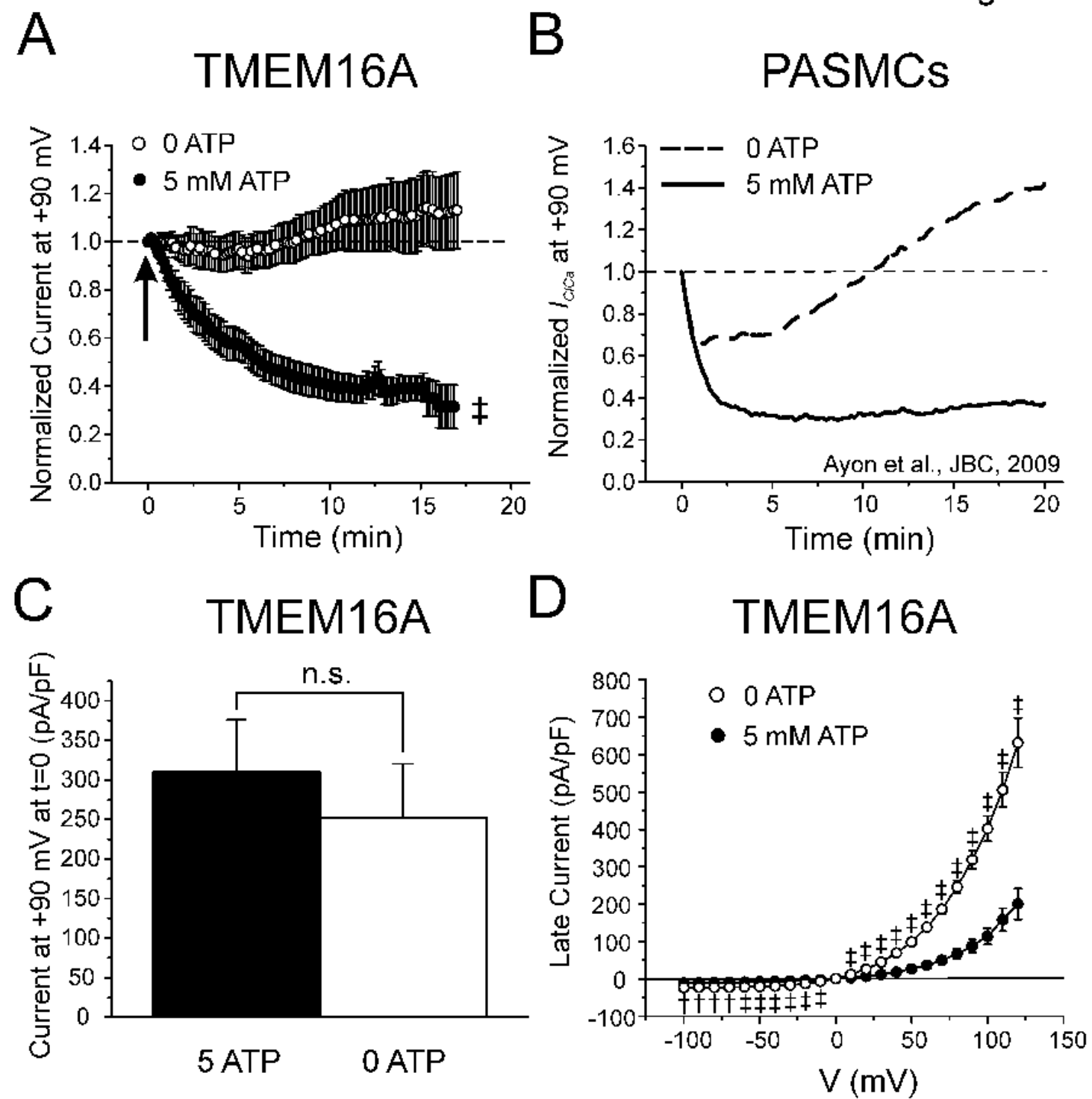
EMI IQFGFVTLFVASFPL APL FALLNNIEIRLDAKKFVTELRRPVAIRAKDI GIWYNILRGVGKLA VIINAFVISFTSDFIPRLVYLYMYSQNGTMHG FVNHTLSSFNVSDFQNGTAPNDPLDLGYEVQICRYKDYREP

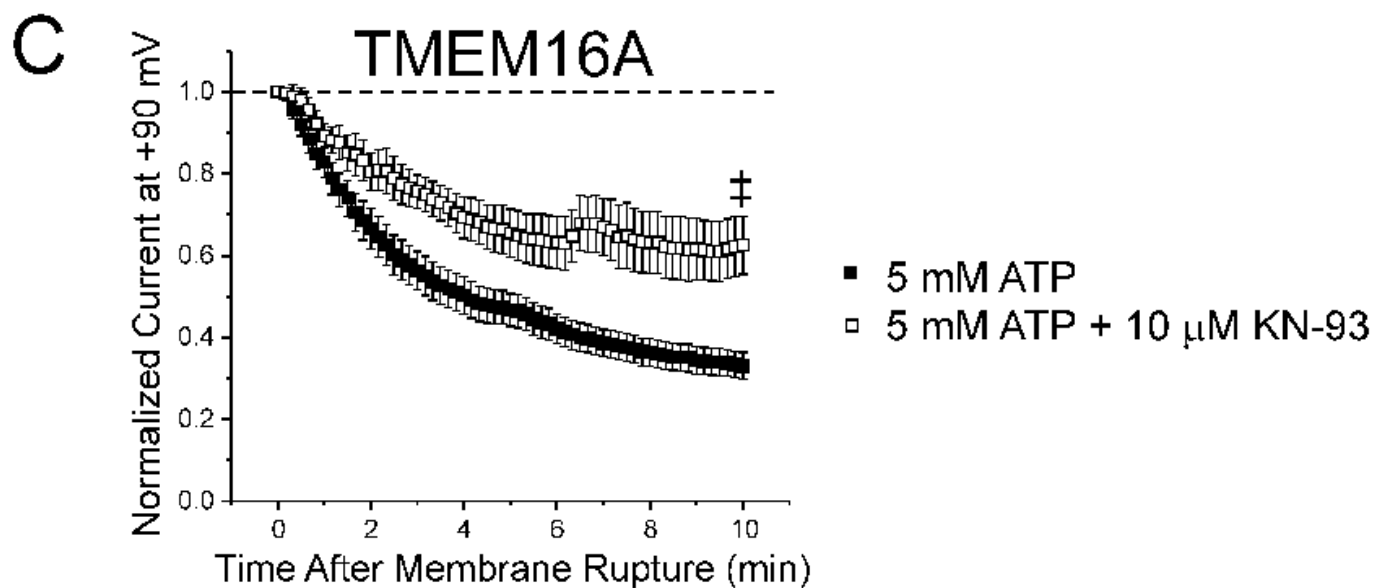
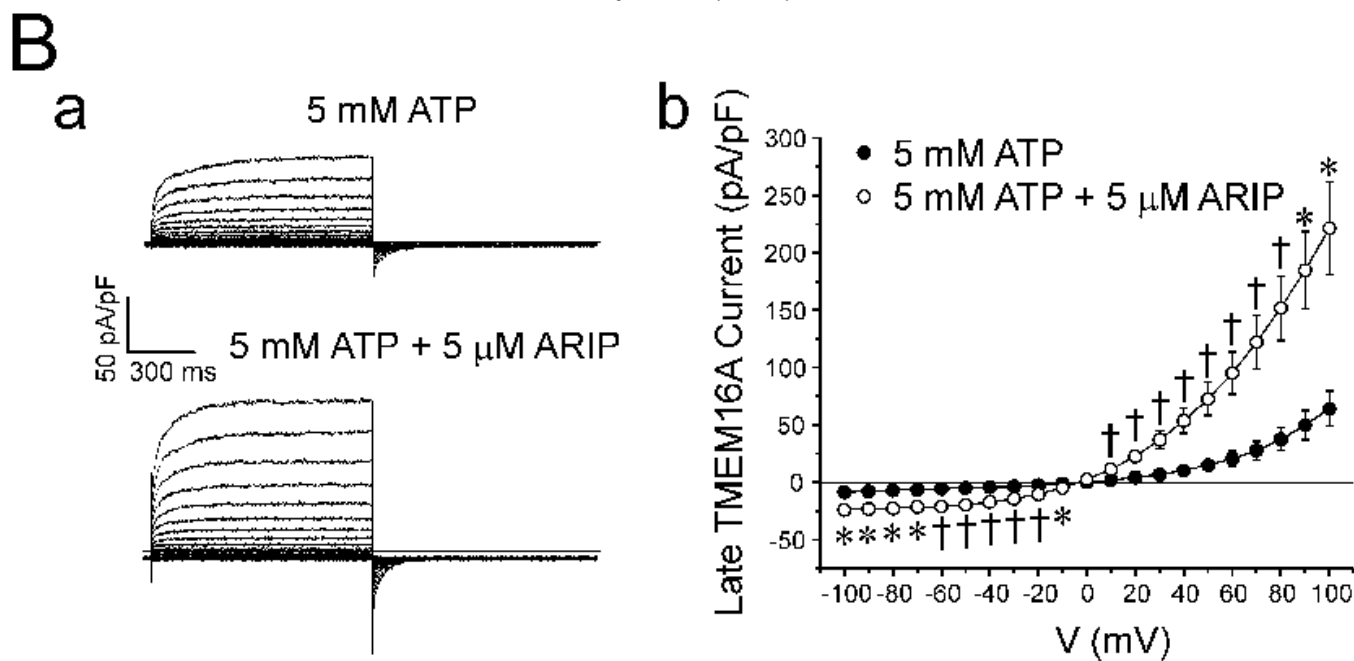
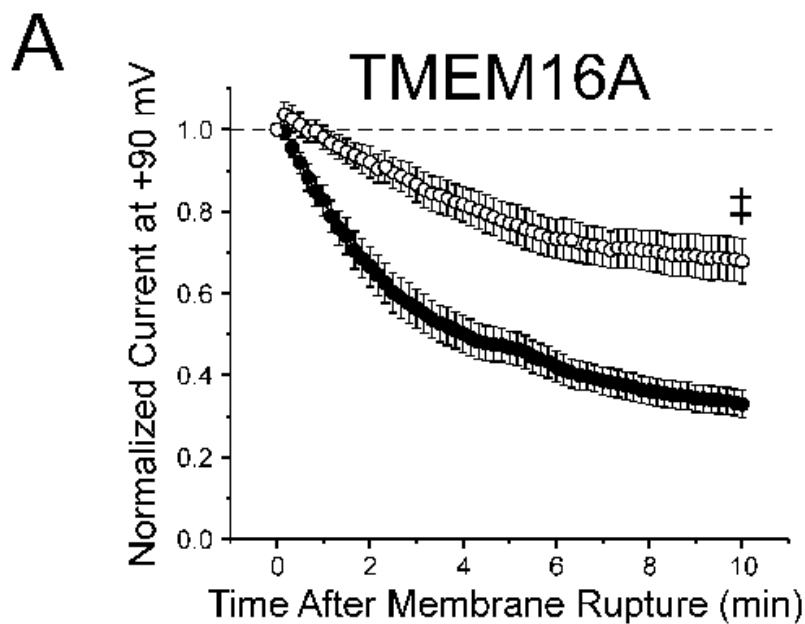
TMD10

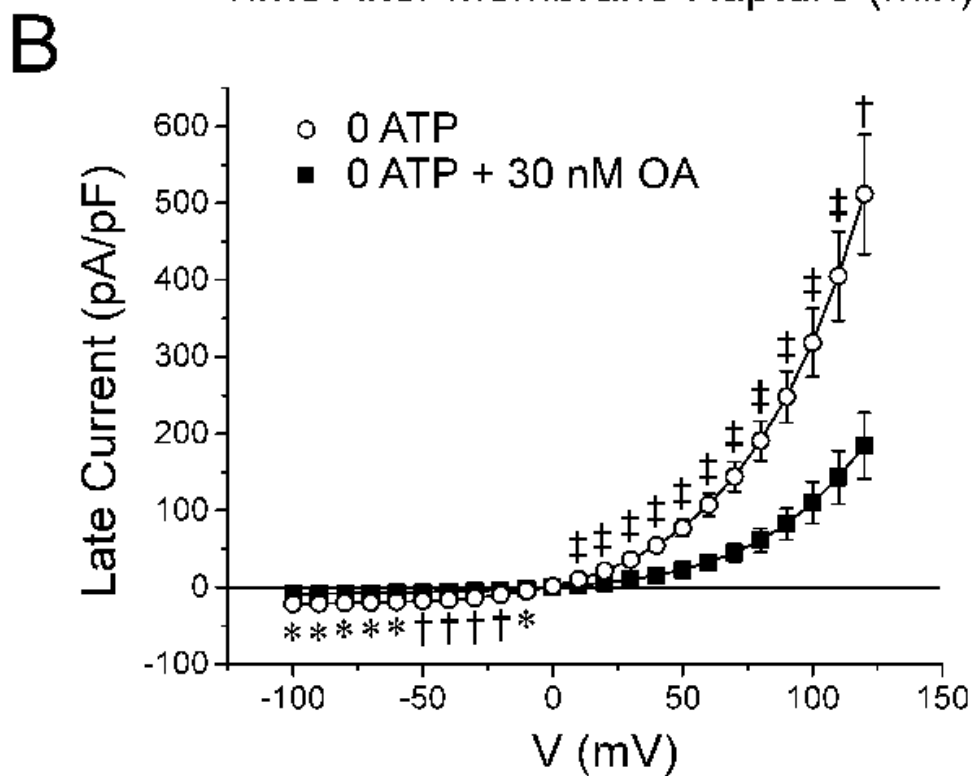
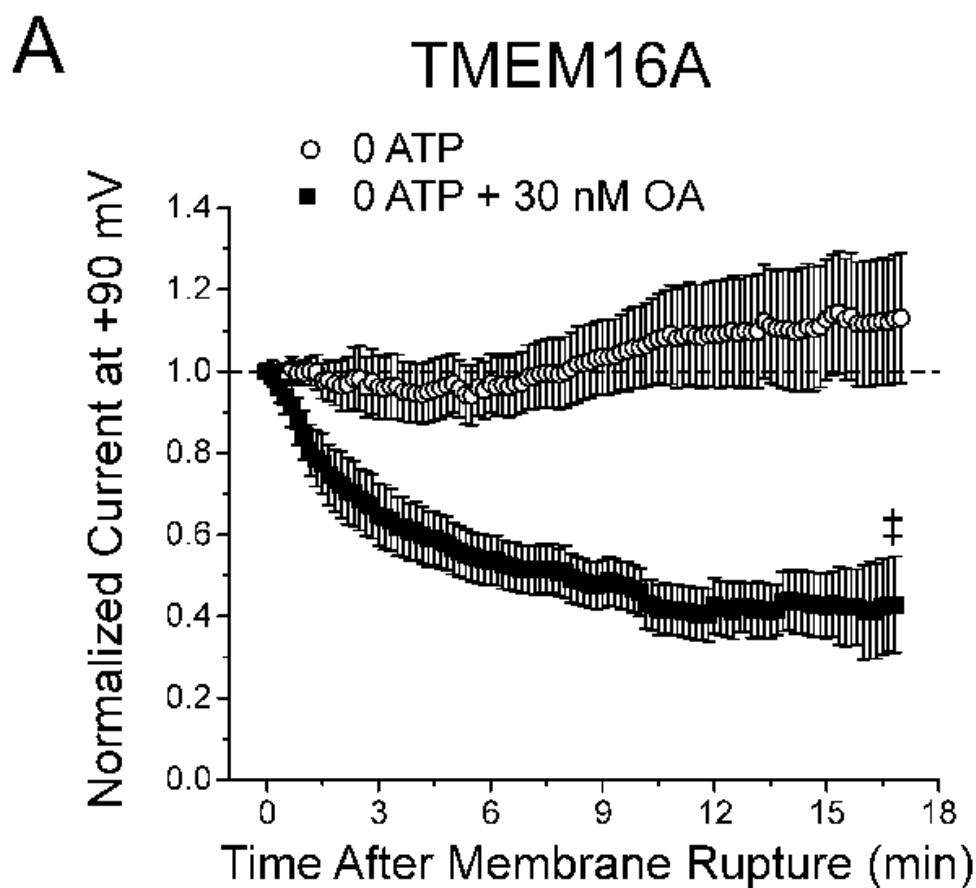
PWSEHKYDIS KDFWAVLAARLAFVIVFONLVMFMSDFVDWVIPDIPKDISQQIHKEKVL MVELFMREEQG

KQQLLDTWMEKEKPRDVPCNNHSPTTHPEAGDGSPVPSYEHGDAL



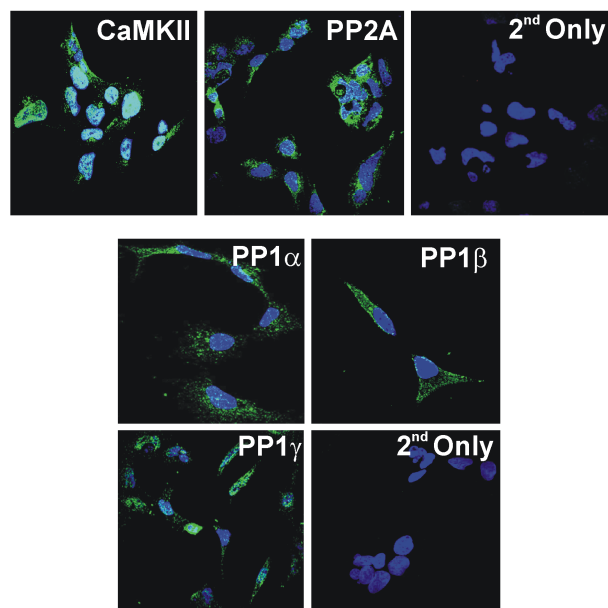




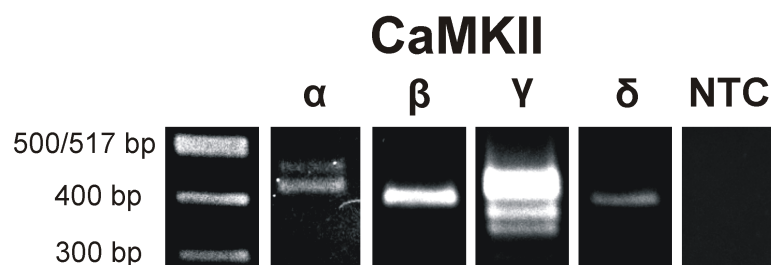


Non-Transfected HEK-293 Cells

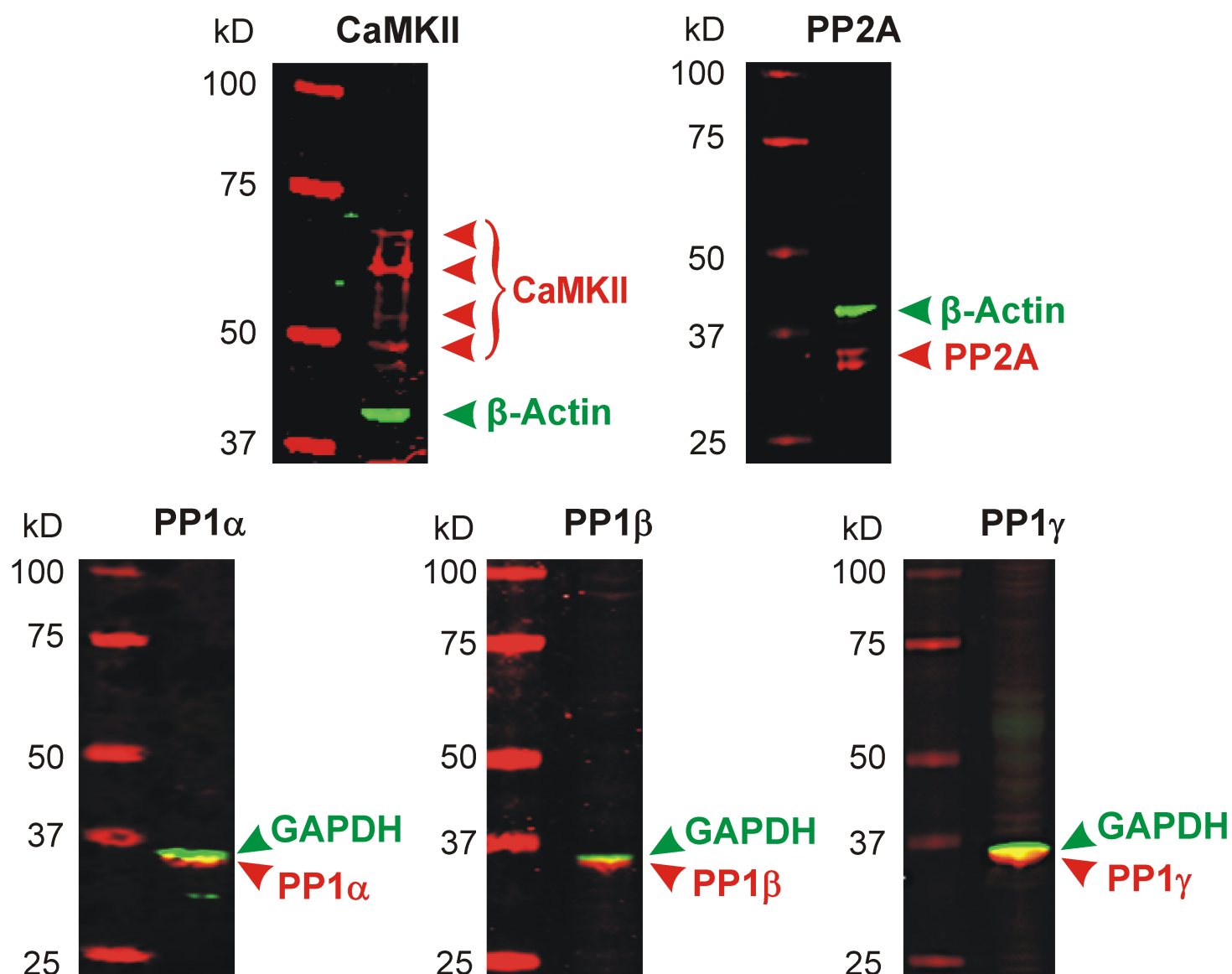
A



B

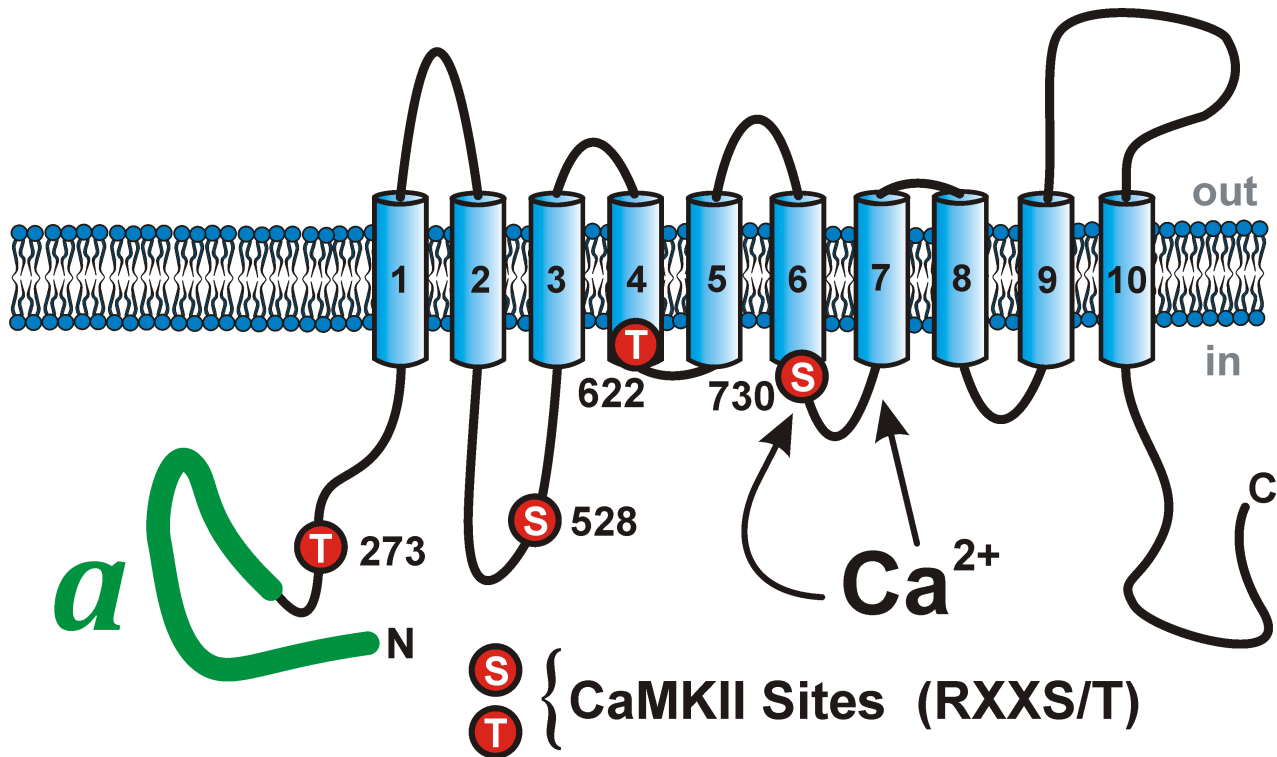


C



A

Mouse TMEM16A-a



B

- X Identical Sequence for Putative CaMKII Site
- X Conservative Replacement
- X Non-Conservative Replacement

CaMKII Site 1 (T273 in mouse):

Mouse (NP_848757.4)	256	QKITDPIQPKVAEH	RPQT	TKRLSYFPSREKQ	286
Rat (NP_001101034.1)	257	QKITDPIQPKVAEH	RPQT	TKRLSYFPSREKQ	287
Human (NP_060513.5)	199	QKITDPIQPKVAEH	RPQT	MKRLSYFPSREKQ	229

CaMKII Site 2 (S528 in mouse):

Mouse (NP_848757.4)	511	PRAEYEARVLEKSL	RKES	RNKETDKVKLTWR	541	
Rat (NP_001101034.1)	534	PRAEYEARVLEKSL	RKES	RNKETDKVKLTWR	564	
Human (NP_060513.5)	454	PRAEYEARVLEKSL	KKES	RNKE	KRRHIPEES	484

↑
Splice Variant *d*

CaMKII Site 3 (T622 in mouse):

Mouse (NP_848757.4)	605	VVIILLDEVYGCIA	RWLT	KIEVPKTEKSFEE	635
Rat (NP_001101034.1)	628	VVIILLDEVYGCIA	RWLT	KIEVPKTEKSFEE	658
Human (NP_060513.5)	574	VVIILLDEVYGCIA	RWLT	KIEVPKTEKSFEE	604

CaMKII Site 4 (S730 in mouse):

Mouse (NP_848757.4)	713	GIPKMKKFIRYLKL	RRQS	PSDREEYVKKRQR	743								
Rat (NP_001101034.1)	736	GIPKMKKFIRYLKL	RRQS	PSDREEY	L	KKRQR	766						
Human (NP_060513.5)	682	GIPKMKK	L	IRYLKL	KQQS	P	D	H	E	E	C	VKKRQR	712

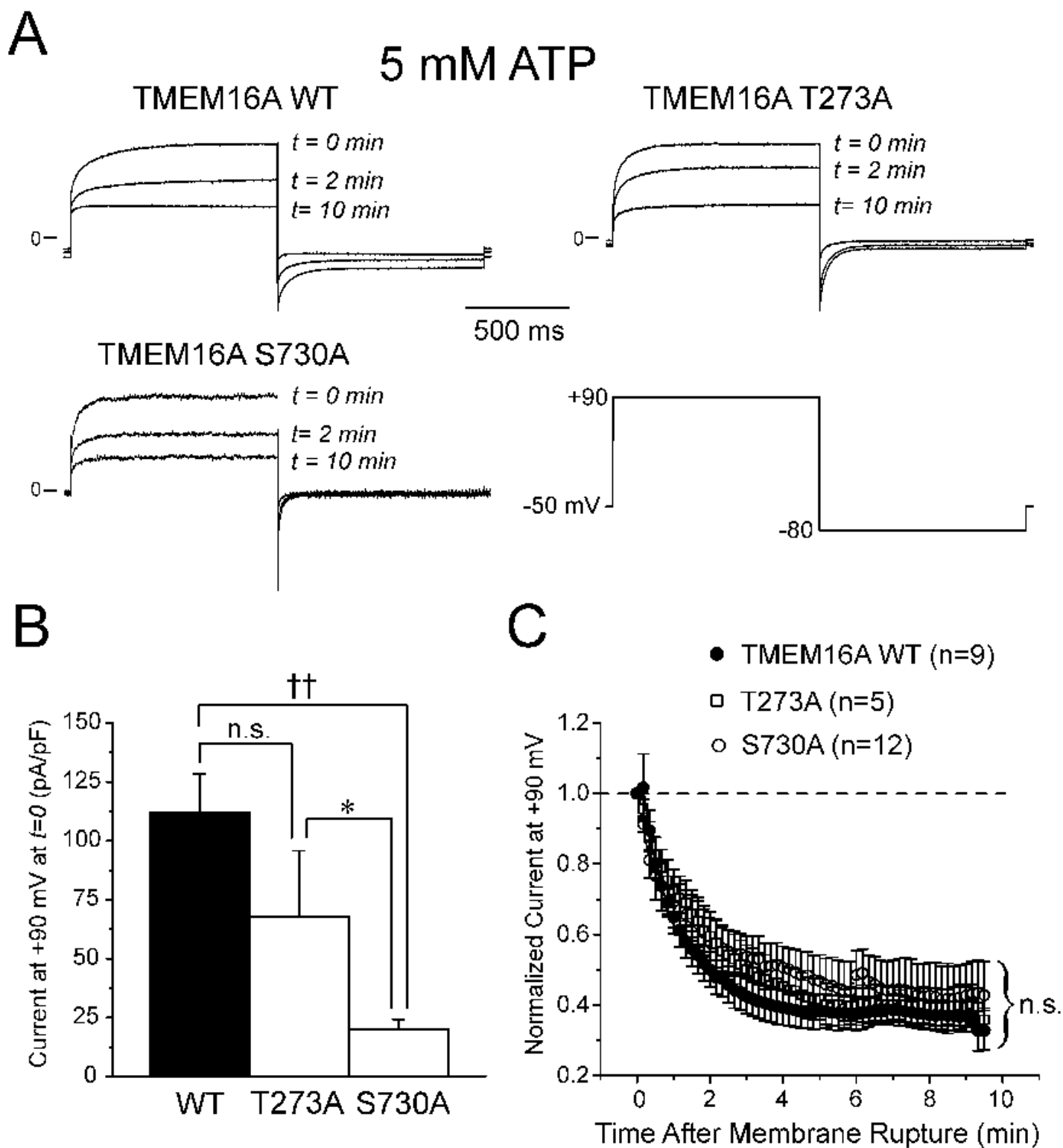


Figure 9

